國 立 交 通 大 學

電信工程學系碩士班

碩士論文

適用於多頻帶正交分頻多工系統之通道

及多微網衍生干擾對抗技術

Channel and Multi-Piconet Induced Interference

Mitigation for Multi-band OFDM System

研 究 生：洪宗樺　　Student: Chung-Hua Hung

指導教授：李大嵩 博士　　Advisor: Dr. Ta-Sung Lee

中 華 民 國 九 十 四 年 六 月

適用於多頻帶正交分頻多工系統之通道及多微網衍生干擾對抗技術

Channel and Multi-Piconet Induced Interference Mitigation for Multi-band OFDM System

研 究 生：洪宗樺　　Student: Chung-Hua Hung

指導教授：李大嵩 博士　　Advisor: Dr. Ta-Sung Lee

國立交通大學

電信工程學系碩士班

碩士論文

A Thesis
Submitted to Institute of Communication Engineering
College of Electrical Engineering and Computer Science
National Chiao Tung University
in Partial Fulfillment of the Requirements
for the Degree of
Master of Science
in
Communication Engineering
June 2005
Hsinchu, Taiwan, Republic of China

中 華 民 國 九 十 四 年 六 月

適用於多頻帶正交分頻多工系統之通道及多微網衍生干擾對抗技術

學生：洪宗樺　　指導教授：李大嵩 博士

國立交通大學電信工程學系碩士班

摘要

由於超寬頻通訊系統具有取代家庭與辦公室內高傳輸速率之有線系統的能力而成為極具潛能的新技術。超寬頻技術可提供每秒數億位元的傳輸速率而其涵蓋的範圍可達數公尺。IEEE802.15.3a 多頻段正交分頻多工(Multiband OFDM, MB OFDM)系統是眾多超寬頻技術中較新的技術之一，該系統每次傳輸只利用 500 MHz 的頻寬並且將該頻寬分割成數個更小的副載波，然而 MB OFDM 之系統效能會受到長延遲擴散通道及多微網間干擾的影響而大幅下降。在本論文中，吾人提出一種具有對抗因長延遲擴散通道產生的載波間干擾(intercarrier interference)及避免其它微網(piconet)干擾之接收機，雖然最小均方差等化器可以改善此 ICI 問題，然而其複雜度過高不利於被 MB OFDM 所採用，因此吾人提出「載波間干擾消除輔助決策法」有效改善此一問題。另一方面，為了降低多微網間之干擾，MB OFDM 採用四組時頻交錯碼，吾人針對此問題提出「避免干擾傳輸法」，此方法略過被干擾的頻槽(frequency slot)，而只在不受干擾的頻槽傳輸信號，藉以達到避免干擾之目的。吾人藉由電腦模擬驗證上述架構在超寬頻環境中可有效改善位元錯誤率。

Channel and Multi-Piconet Induced Interference Mitigation for Multi-band OFDM System

Student: Chung-Hua Hung Advisor: Dr. Ta-Sung Lee

Institute of Communication Engineering

National Chiao Tung University

Abstract

Ultra wideband (UWB) communication is a potential new technique for replacing high-speed data cables in homes and offices. UWB technology will be capable of transmitting hundreds of megabits per second over distances of several meters. Multi-band (MB) orthogonal frequency division multiplexing (OFDM) system is one of the most innovative UWB techniques. MB OFDM system utilizes only 500 MHz instantaneous bandwidth and dividing that frequency band into smaller simultaneously transmitted subcarriers. In this thesis, a MB OFDM receiver is proposed, which mitigates the intercarrier interference (ICI) induced by a long delay spread channel and avoids the interference from other piconet, respectively. Performance of a MB OFDM system is typically significantly degraded due to long delay spread channels. Although the minimum mean-square error (MMSE) equalizer can solve this problem, the matrix inverse computation is too complex for the MB OFDM system. To alleviate this problem, the decision-aided ICI canceller is designed to improve the influence of ICI. On the other hand, the four unique time-frequency interleaving codes are adopted to reduce the effect of cochannel interference (CCI) from simultaneously operating piconets (SOP). Furthermore, we proposed an interference avoidance transmission scheme which turns off the collided frequency slots and conveys signal in the interference-free frequency slots. Finally, we evaluate the performance of the proposed system and confirm that it works well in a UWB environment.

Acknowledgement

I would like to express my deepest gratitude to my advisor, Dr. Ta-Sung Lee, for his enthusiastic guidance and great patience. I learn a lot from his positive attitude in many areas. Heartfelt thanks are also offered to all members in the Communication Signal Processing (CSP) Lab for their constant encouragement. Finally, I would like to show my sincere thanks to my parents and friends for their inspiration and love.

Contents

List of Figures

List of Tables

Acronym Glossary

ADC	analog-to-digital conversion
CAP	contention access period
CCI	cochannel interference
CDMA	code division multiple access
CP	cyclic prefix
CSMA/CA	carrier sense multiple access with collision avoidance
CTAP	channel time allocation period
CTAs	channel time allocations
DAIC	decision-aided ICI canceller
DFT	discrete Fourier transform
DS-UWB	Direct-sequence UWB
FCC	Federal Communications Commission
FCS	frame check sequence
FDMA	frequency division multiple access
FFT	Fast Fourier Transform
FIR	finite impulse response
FSK	frequency shift keying
GPS	global positioning system
HCS	header check sequence
ICI	intercarrier interference
ISI	intersymbol interference
IFFT	Inverse Fast Fourier Transform
LNA	low noise amplifier
LOS	line of sight
LS	least square
LSB	least significant bit
LANs	local-area networks

MAC	Medium Access Control
MB	Multi-band
MCM	multicarrier modulation
MCTAs	management CTAs
MMSE	minimum mean-square error
MPCs	multipath components (MPCs)
NLOS	non-LOS
OFDM	orthogonal frequency division multiplexing
PAPR	peak-to-average power ratio
PHY	Physical Layer
PLCP	physical layer convergence procedure
PNC	piconet coordinator
PSD	power spectral density
QoS	quality of service
QPSK	quadrature phase shift keying
RF	radio frequency
SIR	signal-to-interference ratio
SNR	signal-to-noise ratio
SOP	simultaneously operating piconets
S-V	Saleh-Valenzuela
TDMA	time division multiple access
TFIC	time-frequency interleaving code
TSF	Time Spreading Factor
UWB	Ultra wideband
WLANs	wireless local area networks
WPANs	wireless personal-area networks
ZPP	zero padded prefix

Notations

N_B	number of bands
N_c	number of subcarriers
N_{cp}	number of guard interval samples
N_{DT}	number of data tones
P_{sig}	power of desired signal
P_{int}	power of interference
R	information data rate
T_c	threshold of correlation
T_l	delay of the l^{th} cluster
T_s	symbol duration
W	effective bandwidth of transmitted signal
M	modulation order
X	the lognormal shadowing
α	multipath gain coefficient
$\beta_{k,l}$	fading associated with the k^{th} ray of the l^{th} cluster
Λ	cluster arrival rate
λ	ray arrival rate
τ_κ	delay of the k^{th} multipath component
ρ	correlation coefficient
σ_n^2	noise power
ξ_l	fading associated with the l^{th} cluster

Chapter 1

Introduction

Since the Federal Communications Commission (FCC) approved the regulation for the commercial of Ultra Wideband (UWB) in February 2002, UWB has become a popular technology from commercial or civilian application and the development of UWB technology is drastically gaining momentum recently.

According to FCC definition, any signals that occupy more than 500 MHz bandwidth or have a fractional bandwidth of more than 20% are called UWB. Due to wide bandwidth the signals will be ultra-short waveforms in time domain. As such pulses with ultra-short duration have UWB spectral occupancy, UWB radios possess with some advantages for the radar and communications communities [1]:

1. Strengthened ability to pierce through obstacles
2. Supporting high precision ranging at the few centimeters
3. Providing very high data rates along with a increase in user capacity
4. Potentially small size and processing power

Currently, FCC has allocated 7500 MHz of spectrum for unlicensed use of UWB from 3.1 to 10.6 GHz frequency band and regulates power levels of UWB are very low, which allows UWB technology to overlay already available services such as the global positioning system (GPS) and the IEEE 802.11 wireless local area networks (WLANs) that coexist in the 3.6−10.1 GHz band. According to the

spectrum mask in Figure 1.1 [2], the power spectral density (PSD) measured in 1 MHz bandwidth must not exceed the specified -41.25 dBm [3]. It is a serious challenge to any UWB system about the restriction on PSD because other systems operated in the same band on licensed or unlicensed bands will have a much higher transmitted power than UWB system.

Although there are many challenges to UWB system, UWB is still emerging as a solution for the IEEE 802.15.3a standard [4] due to the properties of the UWB, like low power and high data-rate. The purpose of this standard is to provide a specification for a low complexity, low-cost, low power consumption, and high data-rate wireless connectivity among devices within or entering the personal operating space. The data rate must be high enough (greater than 110 Mbps) to satisfy a set of consumer multimedia industry needs for wireless personal-area networks (WPANs) communications. The standard also addresses the quality of service (QoS) capabilities required to support multimedia data types. Products compliant with this standard are envisioned to complement, not compete with, products compliant with IEEE 802.11 [5] which is a standard for local-area networks (LANs). The difference is similar to the differences between the Ethernet [6] LAN standard and the USB [7] or Firewire [8] standards that provide for connectivity to peripheral devices.

Currently, UWB systems are divided into main two groups: Direct-sequence UWB (DS-UWB) [9]-[11] and Multi-band (MB) OFDM [12]-[14]. In the MB OFDM, the spectrum is divided into several bands and transmits OFDM symbols in all bands. Additionally, in DS-UWB, the spectrum is divided into two sub-bands and the signals using a pseudorandom sequence for the spreading of information bits are transmitted in two sub-bands, respectively.

This thesis is organized as follows. In Chapter 2, we introduce the transmitter architecture of IEEE 802.15.3a MB OFDM system. In Chapter 3, the channel model of UWB and the receiver architecture of the IEEE 802.15.3a MB OFDM system are described. In addition, we introduce the equalization schemes to compensate intercarrier interference (ICI). In Chapter 4, the interference avoidance transmission scheme combining cross-correlator is proposed. In Chapter 5, we conclude this thesis and propose some potential future works.

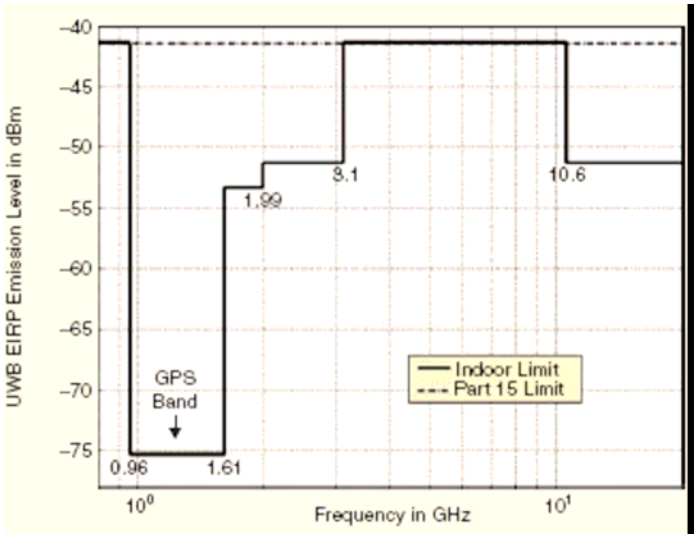

Figure 1.1: UWB spectral mask for indoor communication systems. Emission level is measured in 1 MHz bandwidth.

Chapter 2

Overview of IEEE 802.15.3a Multi-band OFDM System

MB OFDM system is one of the most innovative techniques. MB OFDM system involves utilizing only 500 MHz instantaneous bandwidth and dividing that frequency band into smaller simultaneously transmitted subcarriers. Such systems present high regulatory flexibility for universal operation because they enable independent control of portions of the emitted spectrum to adapt for different environments.

2.1 Review of OFDM

OFDM is a special case of multicarrier transmission, where a single data stream is transmitted over a number of low data rate subcarriers. OFDM can be thought of as a hybrid of multicarrier modulation (MCM) and frequency shift keying (FSK) modulation scheme. The principle of MCM is to transmit data by dividing the data stream into several parallel data streams and modulate each of these data streams onto individual subcarriers. FSK modulation is a technique whereby data is transmitted on one subcarrier from a set of orthogonal subcarriers in symbol duration. Orthogonality between these subcarriers is achieved by separating these subcarriers

by an integer multiples of the inverse of symbol duration of the parallel data streams. With the OFDM technique used, all orthogonal subcarriers are transmitted simultaneously. In other words, the entire allocated channel is occupied through the aggregated sum of the narrow orthogonal subbands.

The main reason to use OFDM systems is to increase the robustness against frequency-selective fading or narrowband interference. In a single carrier system, a single fade or interference can cause the entire link fail, but in a multicarrier system, only a small amount of subcarriers will be affected. Then the error correction coding techniques can be used to correct errors. The equivalent complex baseband OFDM signal can be expressed as

$$x(t)=\begin{cases}\sum_{k=-\frac{N_c}{2}}^{\frac{N_c}{2}-1} d_k\phi_k(t) & 0\le t\le T \\ 0 & \text{Otherwise}\end{cases} = \left[\sum_{k=-\frac{N_c}{2}}^{\frac{N_c}{2}-1} d_k\phi_k(t)\right]u_T(t) \tag{2.1}$$

where N_c is the number of subcarriers, T is the symbol duration, d_k is the transmitted subsymbol (M-PSK or M-QAM), $\phi_k(t)=e^{j2\pi f_k t}/\sqrt{T}$ is the kth subcarrier with the frequency $f_k=k/T$, and $u_T(t)$ is the time windowing function. Using the correlator-based OFDM demodulator, the output of the jth branch can be presented as

$$\begin{aligned} y_j &= \int_0^T x(t)\phi_j^*(t)dt = \frac{1}{T}\sum_{k=-\frac{N_c}{2}}^{\frac{N_c}{2}-1} d_k\int_0^T e^{j2\pi\frac{k-j}{T}t}dt \\ &= d_j \end{aligned} \tag{2.2}$$

By sampling $x(t)$ with the sampling period $T_d=T/N_c$, the discrete time signal x_n can be expressed as

$$x_n = x(t)\big|_{t=nT_d} = \begin{cases}\frac{1}{\sqrt{N_c}}\sum_{k=-\frac{N_c}{2}}^{\frac{N_c}{2}-1} d_k e^{j2\pi\frac{k}{N_c}n} & 0\le n\le N_c-1 \\ 0 & \text{Otherwise}\end{cases} = \text{IFFT}\{d_k\} \tag{2.3}$$

Note that x_n is the Inverse Fast Fourier Transform (IFFT) output of the N input data subsymbols. Similarly, the output of the jth branch can also be presented in the digital form

$$y_j = \mathrm{FFT}\{x_n\} = \frac{1}{\sqrt{N_c}} \sum_{n=0}^{N_c-1} x_k e^{-j2\pi \frac{j}{N_c} n} = \sum_{k=-\frac{N_c}{2}}^{\frac{N_c}{2}-1} x_k \delta[k-j] = d_j \tag{2.4}$$

In theory, the orthogonality of subcarriers in OFDM systems can be maintained and individual subcarriers can be completely separated by the Fast Fourier Transform (FFT) at the receiver when there are no intersymbol interference (ISI) and intercarrier interference (ICI) introduced by transmission channel distortions. However, it is impossible to obtain these conditions in practice. In order to eliminate ISI completely, a guard interval is imposed into each OFDM symbol. The guard interval is chosen larger than the expected delay spread, such that the multipath from one symbol cannot interfere with the next symbol. The guard interval can consist of no signals at all. However, the effect of ICI would arise in that case due to the loss of orthogonality between subcarriers. To eliminate ICI, the OFDM symbol is cyclically extended in the guard interval to introduce cyclic prefix (CP) as shown in Figures 2.1 and 2.2. This ensures that delayed replicas of the OFDM symbol always have an integer number of cycles within the FFT interval, as long as the delay is smaller than the guard interval. As a result, the delayed multipath signals which are smaller than the guard interval will not cause ICI. The complete OFDM signal with CP is given by

$$\tilde{x}_n = \begin{cases} \frac{1}{\sqrt{N_c}} \sum_{k=-\frac{N_c}{2}}^{\frac{N_c}{2}-1} d_k e^{j2\pi \frac{k}{N_c}(n-N_{cp})} & 0 \le n \le N_c + N_{cp} - 1 \\ 0 & \text{Otherwise} \end{cases} \tag{2.5}$$

where N_{cp} is the number of samples in CP. Due to CP, the transmitted OFDM symbol becomes periodic, and the linear convolution process of the transmitted OFDM

symbols with the channel impulse responses will become a circular convolution one. Assuming the value of N_{cp} is larger than the channel length, the received data vector can be expressed as

$$\mathbf{y} = \mathbf{H}\mathbf{x} + \boldsymbol{\eta}$$

$$\underbrace{\begin{bmatrix} y_0 \\ \vdots \\ y_{N_c-1} \end{bmatrix}}_{\mathbf{y}} = \underbrace{\begin{bmatrix} h_0 & 0 & 0 & 0 \\ h_1 & h_0 & 0 & \vdots \\ \vdots & h_1 & \ddots & 0 \\ h_{N_{cp}} & \vdots & \ddots & h_0 \\ 0 & h_{N_{cp}} & \vdots & h_1 \\ \vdots & 0 & \ddots & \vdots \\ 0 & \cdots & 0 & h_{N_{cp}} \end{bmatrix}}_{\mathbf{H}} \underbrace{\begin{bmatrix} x_{-N_c} \\ \vdots \\ x_{-1} \\ x_0 \\ \vdots \\ x_{N_{cp}-1} \end{bmatrix}}_{\mathbf{x}} + \underbrace{\begin{bmatrix} \eta_0 \\ \vdots \\ \eta_{N_c-1} \end{bmatrix}}_{\boldsymbol{\eta}} \tag{2.6}$$

Applying SVD on the channel response, we have

$$\mathbf{H} = \mathbf{U}\boldsymbol{\Sigma}\mathbf{V}^H \tag{2.7}$$

where $\mathbf{U}$ and $\mathbf{V}$ are unitary matrices, and $\boldsymbol{\Sigma}$ is a diagonal matrix. Substituting Equation 2.7 and the equalities of $\mathbf{x} = \mathbf{V}\mathbf{X}$ and $\mathbf{Y} = \mathrm{U}^H\mathbf{y}$ into Equation 2.6, the received data vector can be written as

$$\mathbf{Y} = \mathbf{U}^H\mathbf{y} = \mathbf{U}^H(\mathbf{H}\mathbf{x} + \boldsymbol{\eta}) = \mathbf{U}^H\mathbf{H}\mathbf{V}\mathbf{X} + \underbrace{\mathbf{N}}_{\mathbf{U}^H\boldsymbol{\eta}} = \boldsymbol{\Sigma}\mathbf{X} + \mathbf{N} \tag{2.8}$$

This means that the output $\mathbf{Y}$ can be expressed in terms of the product of $\boldsymbol{\Sigma}$ and $\mathbf{X}$ plus noise. When $x_{-i} = x_{N-i}$ for $i = 1,...,N_{cp}$, a more compact matrix form of the guard interval can be written as

$$\begin{bmatrix} y_0 \\ \vdots \\ y_{N_c-1} \end{bmatrix} = \begin{bmatrix} h_0 & 0 & \cdots & 0 & h_{N_{cp}} & \cdots & h_1 \\ h_1 & h_0 & \ddots & \cdots & 0 & \ddots & \vdots \\ \vdots & h_1 & \ddots & \ddots & \ddots & \ddots & h_{N_{cp}} \\ h_{N_{cp}} & \vdots & \ddots & h_0 & 0 & \cdots & 0 \\ 0 & h_{N_{cp}} & \ddots & h_1 & h_0 & \cdots & \vdots \\ \vdots & \ddots & \ddots & \ddots & \ddots & \ddots & 0 \\ 0 & 0 & \cdots & h_{N_{cp}} & h_{N_{cp}-1} & \cdots & h_0 \end{bmatrix} \begin{bmatrix} x_0 \\ \vdots \\ x_{N_c-1} \end{bmatrix} + \begin{bmatrix} \eta_0 \\ \vdots \\ \eta_{N_c-1} \end{bmatrix} \tag{2.9}$$

where $\mathbf{H}$ becomes a circulant matrix ($\mathbf{H} = \mathbf{Q}^H\boldsymbol{\Lambda}\mathbf{Q}$) and $\mathbf{Q}$ is a discrete Fourier

transform (DFT) matrix with the *l*th entry as

$$\mathbf{Q}_l = \frac{1}{\sqrt{N_c}} e^{-j2\pi \frac{l}{N_c}} \tag{2.10}$$

As in Equation 2.8, the received data **y** can be transformed into **Y**

$$\begin{aligned} \mathbf{Y} &= \mathbf{Q}^H \mathbf{y} = \mathbf{Q}^H (\mathbf{H}\mathbf{x} + \boldsymbol{\eta}) = \underbrace{\mathbf{Q}^H \mathbf{H} \mathbf{Q}^H}_{\boldsymbol{\Sigma}} \mathbf{X} + \underbrace{\mathbf{Q}^H \boldsymbol{\eta}}_{\mathbf{N}} \\ &= \boldsymbol{\Sigma}\mathbf{X} + \mathbf{N} \end{aligned} \tag{2.11}$$

According to Equation 2.11, by adding CP to the OFDM symbol, the modulation in OFDM is equivalent to multiplying the frequency domain signals of the OFDM symbol with the channel's frequency response $\boldsymbol{\Sigma}$.

The block diagrams of the OFDM transceiver is shown in Figure 2.3, where the upper path is the transmitter chain and lower path corresponds to the receiver chain. In the center, IFFT modulates a block of input values onto a number of subcarriers. In the receiver, the subcarriers are demodulated by the FFT, which performs the reverse operation of the IFFT. In fact, the IFFT can be made using the FFT by conjugating input and output of the FFT and dividing the output by the FFT size. This makes it possible to use the same hardware for both transmitter and receiver. This complexity saving is only possible when the transceiver doesn't have to transmit and receive simultaneously. The functions before the IFFT can be discussed as follows. Binary input data is first encoded by a forward error correction code. The encoded data is then interleaved and mapped onto QAM values. In the receiver path, after passing the radio frequency (RF) part and the analog-to-digital conversion (ADC), the digital signal processing starts with a training sequence to determine symbol timing and frequency offset. The FFT is used to demodulate all subcarriers. The FFT outputs are mapped onto binary values and decoded to produce binary output data. In order to successfully map the QAM values onto binary values, the reference phases and amplitudes of all subcarriers have to be acquired first.

In conclusion, OFDM is a powerful modulation technique that simplifies the removal of distortion due to the multipath channel and increases bandwidth efficiency. The key advantages of OFDM transmission scheme can be summarized as follows:

1. OFDM is an efficient way to deal with multipath. For a given delay spread, the implementation complexity is significantly lower than that of a single carrier system with an equalizer.
2. In relatively slow time-varying channels, it is possible to significantly enhance the capacity by adapting the data rate per subcarrier according to the signal-to-noise ratio (SNR) of that particular subcarrier.
3. OFDM is robust against narrowband interference because such interference affects only a small amount of subcarriers.
4. OFDM makes single-frequency networks possible, which is especially attractive for broadcasting applications.

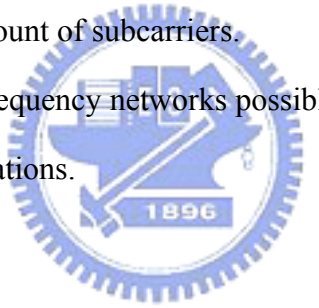

2.2 IEEE 802.15.3a Multi-band OFDM System

The MB OFDM system provides WPANs with data payload communication capabilities of 53.3, 80, 106.7, 160, 200, 320, and 480 Mbps [12]. The support of transmitting and receiving at data rates of 53.3, 106.7, and 200 Mbps are mandatory. The system uses a total of 122 sub-carriers that are modulated using quadrature phase shift keying (QPSK). Forward error correction coding (convolutional coding) is used with a coding rate of 1/3, 1/2, 5/8, and 3/4. The MB OFDM system utilizes a time-frequency interleaving code (TFIC) to interleave coded data over 3 frequency bands (called a band group). Four such band groups with 3 bands each and one band

group with 2 bands are defined. There are also four 3-band TFICs and two 2-band TFICs, which, when combined with the appropriate band groups provide the capability to define eighteen separate logical channels or independent piconets.

2.2.1 PHY Frame Structure

As shown in Figure 2.4, a complete PLCP frame format defined in the MB OFDM standard consists of the PLCP preamble, PLCP header, MAC frame body (frame payload plus FCS), Tail bits and Pad bits. In the Specification, the PLCP preamble includes two kinds of OFDM training signals, which are used for synchronization, carrier-offset recovery, and channel estimation in the receiver, respectively. The PLCP header of the PLCP frame is composed of several fields, and the information conveyed in these fields is processed in the receiver to aid the demodulation from the frame payload.

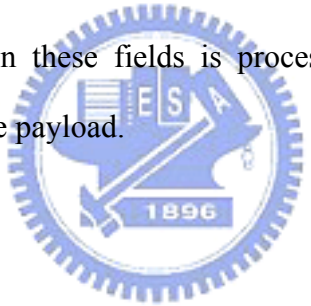

PLCP Preamble Field

There are two kinds of PLCP preamble: standard PLCP preamble and shortened PLCP preamble. The main function of the standard PLCP preamble field is for receiver synchronization, carrier-offset, and channel estimation. The structure of the standard preamble defined in the MB OFDM is shown in Figure 2.5. The standard preamble includes three distinct portions: packet synchronization sequence, frame synchronization sequence, and channel estimation sequence. The packet synchronization sequence is composed of successively 21 repetitions of a time-domain sequence. Each period of the timing synchronization sequence is constructed by appending 37 “zero samples” to the sequences. This portion of the standard preamble is used for packet detection, acquisition, coarse carrier frequency estimation, and coarse symbol timing. The frame synchronization sequence of the

preamble is composed of successively 3 repetitions of a time-domain sequence similar to the packet synchronization sequence. This portion of the standard preamble is used to synchronize the receiver algorithm within the preamble. Finally, the channel estimation sequence of the standard preamble is composed of successively 6 repetitions of the OFDM training symbol. This training symbol is generated by passing the frequency-domain sequence though the IFFT, and appending the output with 37 “zero samples” to the resulting time-domain output. This portion of the standard preamble is used to estimation the channel frequency response, fine carrier frequency estimation, and fine symbol timing.

For data rates of 200 Mbps and lower, all the packets use the standard PLCP preamble. However, for the data rates higher than 200 Mbps, the first packet use the standard PLCP preamble, while the remaining packets use the shortened PLCP preamble. The structure of the shortened preamble is shown in Figure 2.6.

PLCP Header

As show in Figure 2.4, The PLCP header composed of PHY header and MAC header is always sent at an information data rate of 53.3 Mbps. The bit assignment of PHY header is illustrated in Figure 2.7. The RATE field occupies the Bits 2-6 of the PHY header, and conveys the information about the data rate chosen to transmit the following MAC frame body. The mapping between the data rate and the content of the RATE field is shown in Table 2.1. By the information from the RATE field, the receiver can determine what coding rate of the FEC coding is used in MAC frame body. Bits 9-20 of the PHY header are the LENGTH field, and the information conveyed in this field indicates the number of octets in MAC frame body. The number of octets in the LENGTH field shall be an unsigned 12-bit integer and has the range from 1 to 4095, and the least significant bit (LSB) shall be transmitted first

in time. Bit 23-24 shall encode the initial state of the scrambler, which is used to synchronize the descrambler of the receiver. For the other bits of PHY header, these are reversed for future use. The Tail bits are added after the PHY header in order to return the convolutional encoder to the “zero state”. Because the information conveyed in the RATE, LENGTH and SCRAMBLER fields are required for coding MAC frame body, it is required that these fields can be decoded immediately after the reception of the Tail field. Pad bits are added to the end of the Tail bits in order to align the data stream in the OFDM symbol interleaver boundaries. The remainder of the PLCP frame is sent at the desired information data rate depended on modulation parameter listed in Table 2.2.

2.2.2 Transmitter Architecture

As show in Figure 2.9, the transmitter architecture of MB OFDM is similar to that of a conventional OFDM system. In the following section we will introduce the transmitter architecture of MB OFDM in detail [13][14].

Data Scrambler

This is a method of removing long runs of 0’s or 1’s in the signal which would otherwise give the receiver a problem at the other end of the channel. This is achieved at the bit level. The MAC header, HCS, and MAC frame body are scrambled according to the scrambler seed identifier. However, the PLCP preamble, PLCP header, and tail bits shall not be scrambled. Because the initialization vector is determined from the seed identifier contained in the PLCP header of the received frame. The polynomial generator, $g(D)$, for the pseudo random binary sequence (PRBS) generator shall be $g(D) = 1 + D^{14} + D^{15}$, where D is a single bit delay element. the corresponding PRBS, x_n, is generated as

$$x_n = x_{n-14} \oplus x_{n-15} \tag{2.12}$$

where "⊕" denotes modulo-2 addition. This is realized, as shown in Figure 2.9, with a shift register. The following sequence defines the initialization sequence, x_{init}, which is specified by the parameter "seed value" in Table 2.3.

$$x_{init} = [x_{n-1}^{i} \quad x_{n-2}^{i} \quad \cdots \quad x_{n-14}^{i} \quad x_{n-15}^{i}] \tag{2.13}$$

where x_{n-k}^{i} represents the binary initial value at the output of the kth delay element. The scrambled data bits, s_n, are obtained as follows:

$$s_n = b_n \oplus x_n \tag{2.14}$$

where b_n represents the unscrambled data bits. The de-scrambler at the receiver shall be initialized with the same initialization vector, x_{init}, used in the transmitter scrambler. The 15-bit seed value shall correspond to the seed identifier as shown in Table 2.3.

Convolutional Encoder

Convolutional coding operates at the bit level rather than block level such as RS coding. This has the advantage of the generator not having to store a whole block of data in expensive memory prior to performing the coding. The input stream is fed into shift register stages which have intermediate output taps after each stage. The input stream and various output taps are modulo two added. The MB OFDM system actually uses 6 shift register stages and the rate R = 1/3 with the generator polynomials are shown as,

$G_0 = 133_{Oct}$, $G_1 = 145_{Oct}$ and $G_2 = 175_{Oct}$

The architecture ,as shown in Figure 2.10, can be considered a state machine. Since there are 6 stages in the MB OFDM implementation, this gives rise to 64 states. It is the change from one state to another based on which we can draw the trellis diagram to be applied in the Viterbi decoding algorithm.

The various coding rates are derived from the rate R = 1/3 convolutional code by employing “puncturing”. Puncturing is a procedure for deleting the selected encoded bits in the transmitter (thus the number of transmitted bits are reduced and the coding rate is increacsed) and inserting a dummy “zero” metric into the convolutional decoder on the receive side according to the omitted bits pattern. The puncturing patterns are illustrated in Figures 2.11- 2.13. In each of these cases, the tables shall be filled in with encoder output bits from the left to the right. For the last block of bits, the process shall be stopped at the point at which encoder output bits are exhausted, and the puncturing pattern applied to the partially filled block. The PHY header, tail bits, MAC header, HCS, tail and pad bits shall be coded with a rate R = 1/3. The encoder shall be reset to the all-zero state following this. Next, the MAC frame body and tail bits shall be coded with a rate R = 1/3, 1/2, 5/8, or 3/4, corresponding to the desired data rate.

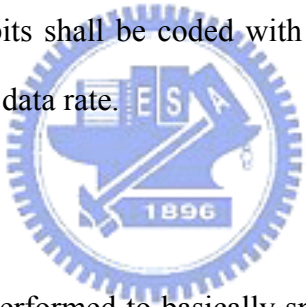

Bit interleaving

Bit interleaver is also performed to basically spread out the errors and so make the convolutional coding more effective. Bit interleaving provides robustness against burst errors. The bit interleaving operation is performed in three stages: (i) symbol interleaving across the OFDM symbols, (ii) intra-symbol tone interleaving, and (iii) intra-symbol cyclic shifts. The symbol interleaver permutes the bits across OFDM symbols to exploit frequency diversity across the sub-bands, while the tone interleaver permutes the bits across the data tones within an OFDM symbol to exploit frequency diversity across tones and provide robustness against narrow-band interferers. The length of the symbol interleaver is determined by the Time Spreading Factor (TSF) defined in Table 2.2. The symbol interleaver shall interleave among (6/TSF)*N_{CBPS} coded bits, where N_{CBPS} is the number of coded bits per OFDM

symbol. Following this, the symbols shall each be cyclically shifted by a different amount as described further in this section. This is done to exploit frequency diversity, especially in the modes that do not employ time spreading.

For the bit interleaving operation, the coded bits shall first be grouped together into blocks of (6/TSF)*N_{CBPS} coded bits. Each group of coded bits shall then be permuted using a block interleaver of size (6/TSF)*N_{CBPS}. Let the sequences $\{U(i)\}$ and $\{S(i)\}$, where i = 0,…, (6/TSF)*N_{CBPS}−1, represent the input and output bits of the symbol block interleaver, respectively. The input-output relationship of this interleaver shall be given by:

$$S(i) = U\left\{\text{Floor}\left(\frac{i}{N_{CBPS}}\right) + (6/TSF) * \text{Mod}(i, N_{CBPS})\right\} \tag{2.15}$$

where the function Floor(·) returns the largest integer value less than or equal to its argument value, and where the function Mod(·) returns the remainder after division of i by N_{CBPS}.

The output of the symbol block interleaver is then passed through a tone block interleaver. The outputs of the symbol block interleaver are grouped together into blocks of N_{CBPS} bits and then permuted using a regular block interleaver of size N_{Tint} × 10, where N_{Tint} = N_{CBPS}/10. Let the sequences $\{S(i)\}$ and $\{T(i)\}$, where i = 0,…, N_{CBPS}−1, represent the input and output bits of the tone interleaver, respectively. The input-output relationship of the tone block interleaver is given by:

$$T(i) = S\left\{\text{Floor}\left(\frac{i}{N_{T\,\text{int}}}\right) + 10 * \text{Mod}(i, N_{T\,\text{int}})\right\} \tag{2.16}$$

where the function Mod(·) returns the remainder after division of i by N_{Tint} .

The output of the tone interleaver is then passed through the last stage, which consists of a different cyclic shift of each block of N_{CBPS} bits within the span of the symbol interleaver defined above. Let $\{T(b,i)\}$ and $\{V(b,i)\}$, where i =

0,1,…,N_{CBPS}−1, represent the input and output sequences, respectively, of the cyclic shift for the bth block. Then,

$$V(b,i) = T\left(b, \mathrm{Mod}(i + A(b), N_{CBPS})\right) \tag{2.17}$$

For conjugate symmetric modes, N_{CBPS} = 100 : $A(b)$ = b*33, b = 0,1,2. For non-conjugate symmetric modes with time spreading (TSF = 2), N_{CBPS} = 200 : $A(b)$ = b*66, b = 0,1,2. For non-conjugate symmetric modes with no time spreading (TSF=1), N_{CBPS}=200: $A(b)$ = b*33, b = 0,1,2,…,5.

Modulation

The OFDM subcarriers shall be modulated using QPSK. The conversion shall be performed according to the Gray-coded constellation mappings. The output values, d, are formed by multiplying the resulting (I + jQ) value by a normalization factor of K_{MOD}, as described in the following equation:

$$d = (I + jQ) \times K_{\mathrm{MOD}}$$

The normalization factor, K_{MOD}, depends on the base modulation mode, as prescribed in Table 2.4. For QPSK, b_0 determines the I value, and b_1 determines the Q value, as illustrated in Table 2.5.

Frequency-domain Spreading

For information data rates of 53.3 and 80 Mbps, the stream of complex symbols is divided into groups of 50 complex numbers. We shall denote these complex numbers $c_{n,k}$, which corresponds to subcarrier n of OFDM symbol k, as follows:

$$\begin{aligned} c_{n,k} &= d_{n+50*k} \\ c_{(n+50),k} &= d^*_{(49-n)+50*k} \end{aligned} \qquad n = 0,1,...,49,\ \ k = 0,1,...,N_{SYM} - 1 \tag{2.18}$$

where N_{SYM} denotes the number of OFDM symbols in the MAC frame body, Tail bits, and pad bits.

For information data rates of 110, 160, 200, 320, 400 and 480 Mbps, the stream of complex numbers is divided into groups of 100 complex numbers. We shall denote these complex numbers $c_{n,k}$, which corresponds to subcarrier n of OFDM symbol k, as follows:

$$c_{n,k} = d_{n+100*k} \qquad n = 0,1,...,99,\ \ k = 0,1,...,N_{SYM} - 1 \qquad (2.19)$$

where N_{SYM} denotes the number of OFDM symbols in the MAC frame body, Tail bits, and Pad bits.

An OFDM symbol $r_{data,k}(t)$ is defined as

$$\begin{aligned} r_{data,k}(t) = & \sum_{n=0}^{N_{SD}} c_{n,k} \exp(j2\pi M(n)\Delta_F(t - T_{CP})) \\ & + p_{\mathrm{MOD}(k,127)} \sum_{n=-N_{ST}/2}^{N_{ST}/2} P_n \exp(j2\pi n\Delta_F(t - T_{CP})) \end{aligned} \qquad (2.20)$$

where N_{SD} is the number of data subcarriers, N_{ST} is the number of total subcarriers, and p_{MOD} and P_n together describe the contribution of the pilot and guard subcarriers, as further defined in Pilot Subcarriers section. The function M(n) defines a mapping from the indices 0 to 99 to the logical frequency offset indices –56 to 56, excluding the locations reserved for the pilot subcarriers, guard subcarriers, and the DC subcarrier, as shown below:

$$M(n)=\begin{cases} n-56 & n=0 \\ n-55 & 1\le n\le 9 \\ n-54 & 10\le n\le 18 \\ n-53 & 19\le n\le 27 \\ n-52 & 28\le n\le 36 \\ n-51 & 37\le n\le 45 \\ n-50 & 46\le n\le 49 \\ n-49 & 50\le n\le 53 \\ n-48 & 54\le n\le 62 \\ n-47 & 63\le n\le 71 \\ n-46 & 72\le n\le 80 \\ n-45 & 81\le n\le 89 \\ n-44 & 90\le n\le 98 \\ n-43 & n=99 \end{cases} \tag{2.21}$$

Pilot Subcarriers

In each OFDM symbol following the PLCP preamble, twelve of the subcarriers are dedicated to pilot signals in order to make coherent detection robust against frequency offsets and phase noise. These pilot signals shall be put in subcarriers numbered –55, –45, –35, –25, –15 –5, 5, 15, 25, 35, 45, and 55. The contribution due to the pilot subcarriers for the k^{th} OFDM symbol is given by the inverse Fourier Transform of the sequence $P_{n,k}$ below, which includes BPSK modulation by a pseudorandom binary sequence, p_l (defined further below), to prevent the generation of spectral lines.

$$P_n = p_{\text{MOD}(k,127)}\begin{cases} \dfrac{1+j}{\sqrt{2}} & n=15,45 \\ \dfrac{-1-j}{\sqrt{2}} & n=5,25,35,55 \\ 0 & n=\pm 1\ldots,\pm 4,,\pm 6,\ldots,\pm 14,\pm 16,\ldots,\pm 24, \\ & \quad \pm 26,\ldots,\pm 34,\pm 36,\ldots,\pm 44,\pm 46,\ldots,\pm 54,\pm 56 \end{cases} \tag{2.22}$$

For modes with data rates less than 106.7 Mbps:

$$P_{n,k} = P^{*}_{-n,k}, \qquad n=-5,-15,-25,-35,-45,-55 \tag{2.23}$$

For 106.7 Mbps and all higher rate modes:

$$P_{n,k} = P_{-n,k}, \qquad n = -5,-15,-25,-35,-45,-55 \qquad (2.24)$$

In this numbering, k = 0 shall correspond to the first OFDM symbol following the PLCP preamble. The length 127 pseudo-random sequence, p_l, which modulates the pilot subcarriers is defined below:

$p_{0\ldots126}$ = {1, 1, 1, 1, -1, -1, -1, 1, -1, -1, -1, -1, 1, 1, -1, 1, -1, -1, 1, 1, -1, 1, 1, -1, 1,
1, 1, 1, 1, 1, -1, 1, 1, 1, -1, 1, 1, -1, -1, 1, 1, 1, -1, 1, -1, -1, -1, 1, -1, 1, -1, -1, 1, -1,
-1, 1, 1, 1, 1, 1, -1, -1, 1, 1, -1, -1, 1, -1, 1, -1, 1, 1, -1, -1, -1, 1, 1, -1, -1, -1, -1, 1,
-1, -1, 1, -1, 1, 1, 1, 1, -1, 1, -1, 1, -1, 1, -1, -1, -1, -1, -1, 1, -1, 1, 1, -1, 1, -1, 1, 1,
1, -1, -1, 1, -1, -1, -1, 1, 1, 1, -1, -1, -1, -1, -1, -1, -1}.

Guard Subcarriers

In each OFDM symbol ten of the subcarriers at the edges of the occupied frequency band shall be termed guard subcarriers. There are five guard subcarriers on either edge of the OFDM symbol occupied band, located in subcarriers with indices –61, –60, …, –57, and 57, 58, …, 61. These guard subcarriers shall be created by copying over the five outermost data-bearing subcarriers from the nearest edge of the OFDM symbol as shown in Figure 2.14 (note the intervening pilot subcarrier is not copied). The guard subcarrier symbol definition for the nth subcarrier of the kth symbol shall be given as follows:

$$\begin{aligned} P_{n,k} &= c_{m,k},\ l = 0,1,2,3,4;\ n = 57 + l;\ m = 95 + l \\ P_{n,k} &= c_{m,k},\ l = 0,1,2,3,4;\ n = -61 + l;\ m = l \end{aligned} \qquad (2.25)$$

In this numbering, k = 0 shall correspond to the first OFDM symbol following the PLCP preamble (i.e., the first OFDM symbol following the channel estimation symbols).

Time-domain Spreading

For data rates of 53.3, 80, 110, 160 and 200 Mbps a time-domain spreading operation shall be performed with a spreading factor TSF = 2, in order to improve frequency diversity and Simultaneously Operating Piconets (SOP) performance. The time-domain spreading shall consist of transmitting the same information over two OFDM symbols. The *k*th original OFDM symbol, represented as $S_k(l)$, shall be generated as specified in Modulation section. The repeated version of this OFDM symbol, represented as $S_k^{'}(l)$, shall be obtained in the time domain as follows:

$$S_k^{'}(l) = \begin{cases} \left\{ \mathrm{Im}\left\{S_k(l)\right\} + j\,\mathrm{Re}\left\{S_k(l)\right\} \right\} p_{\mathrm{Mod(k+6,127)}} & \text{no conjugate symmetry} \\ S_k(l)\, p_{\mathrm{Mod(k+6,127)}} & \text{with conjugate symmetry} \end{cases} \quad (2.26)$$

where k = 0 shall correspond to the first OFDM symbol following the PLCP preamble, i.e., the first OFDM symbol following the channel estimation symbols, and the values of the index k are OFDM symbol numbers before time spreading. Also, the values for p_k are selected from the same pseudo-random sequence used to scramble the pilot subcarriers.

Operating Band Frequency

The MB OFDM system defines a unique numbering system for all channels that have a spacing of 528 MHz and lie within the band 3.1-10.6 GHz. The relationship between center frequency and band number is

$$\text{Band center frequency} = 2904 + 528 \times n_b, n_b = 1...14\,(\text{MHz}) \quad (2.27)$$

as shown in Figure 2.15 and based on Equation 2.27, five band groups are defined, consisting of four groups of three bands and one group of two bands as shown in Table 2.6.

2.3 Summary

The Specification of MB OFDM system has been introduced in this chapter. Although the transmitter architecture is similar to conventional OFDM system, some properties of channel are induced by the ultra wide bandwidth waveforms and some receiver function blocks should be modified. The following details will be discussed in Chapter 3.

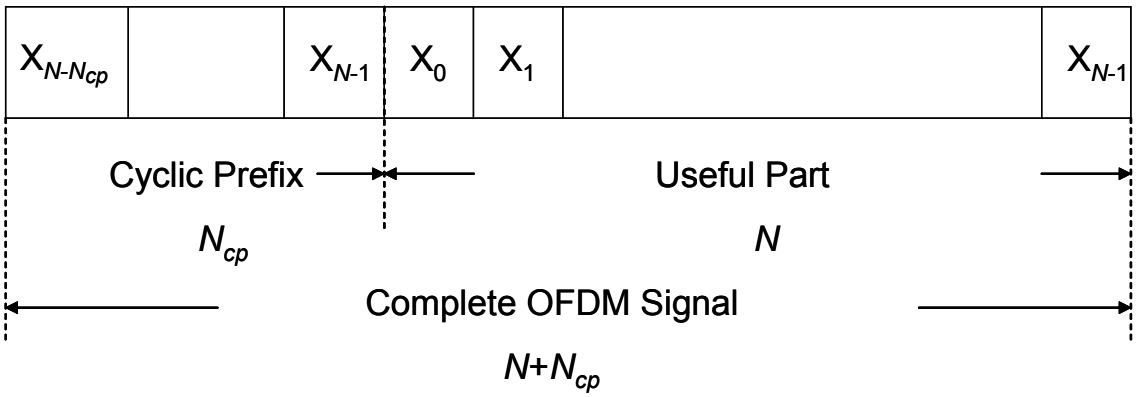

Figure 2.1: OFDM signal with cyclic prefix extension.

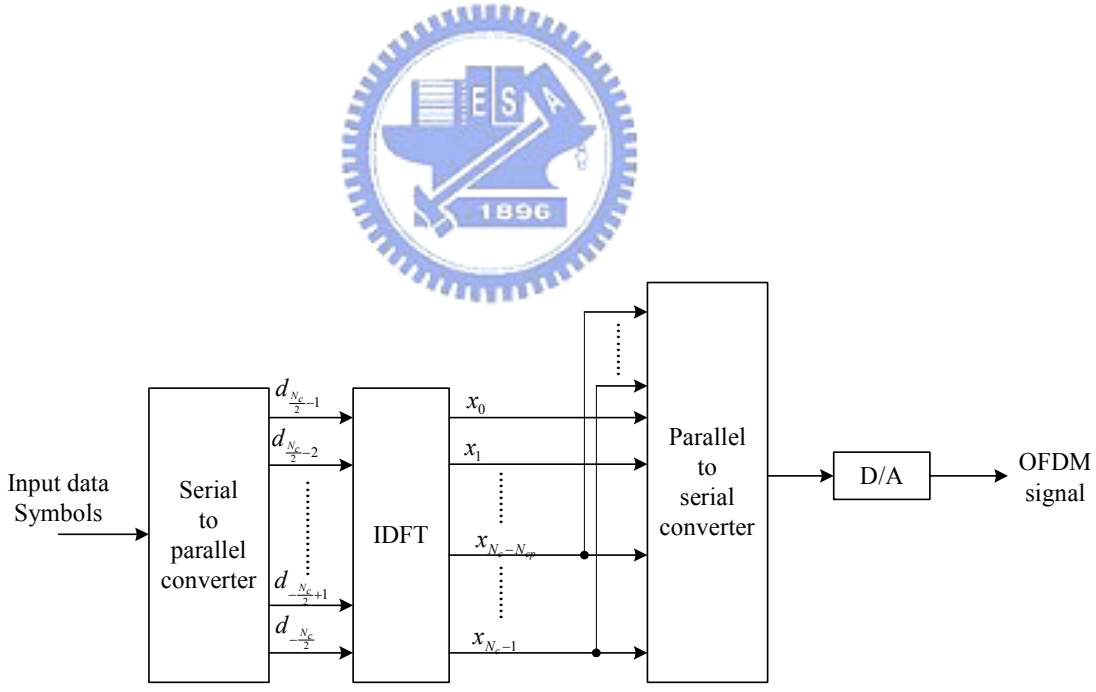

Figure 2.2: A digital implementation of appending cyclic prefix into the OFDM signal in the transmitter.

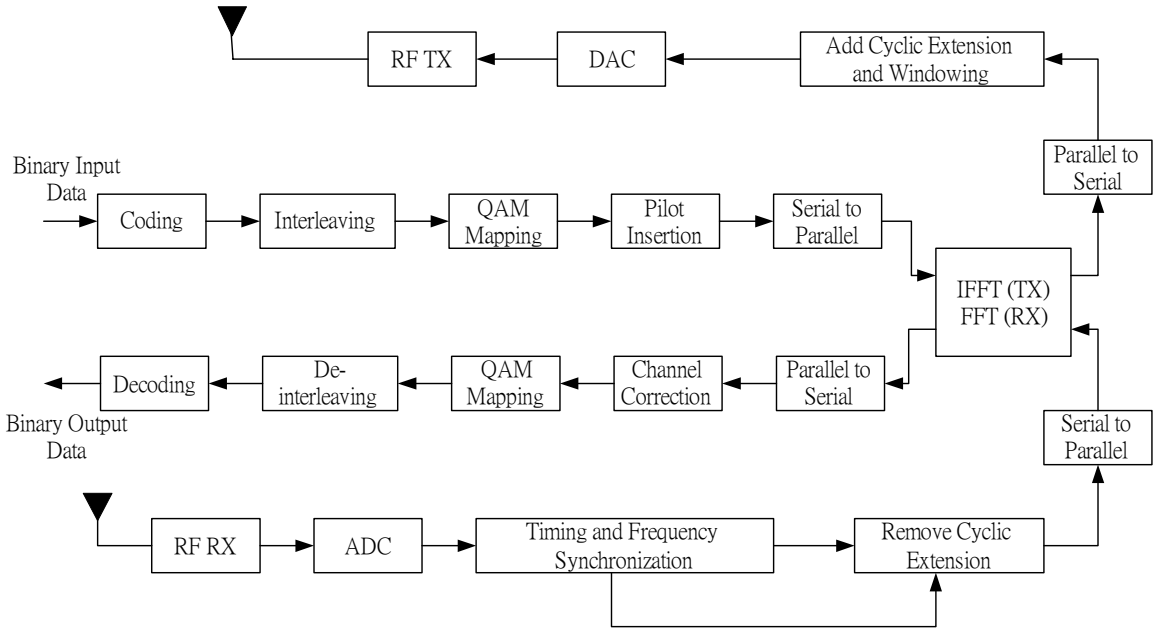

Figure 2.3: Black diagrams of the OFDM transceiver.

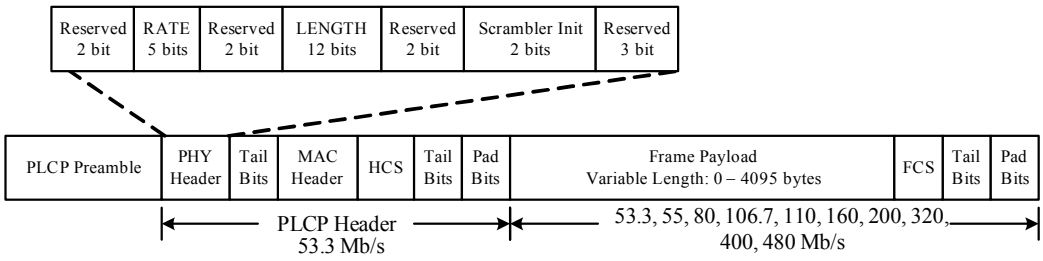

Figure 2.4: PLCP frame format of the MB OFDM system.

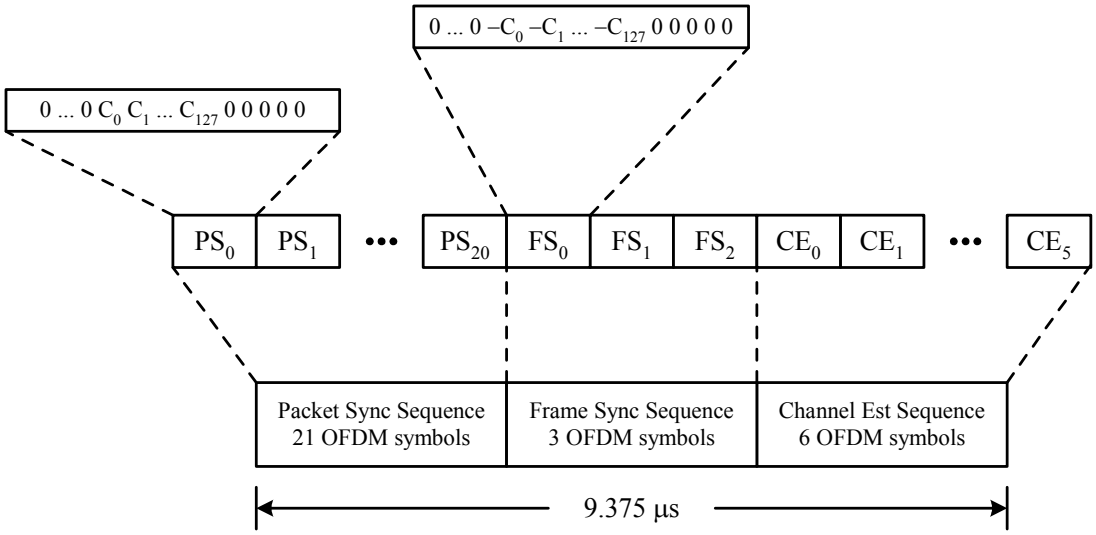

Figure 2.5: Standard PLCP preamble format of the MB OFDM system

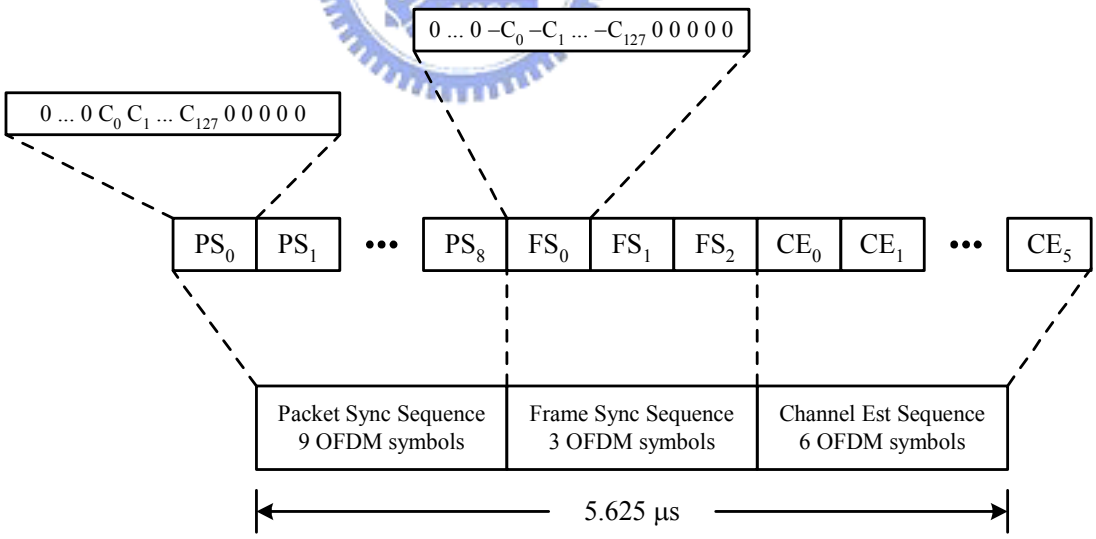

Figure 2.6: Shortened PLCP preamble format of the MB OFDM system

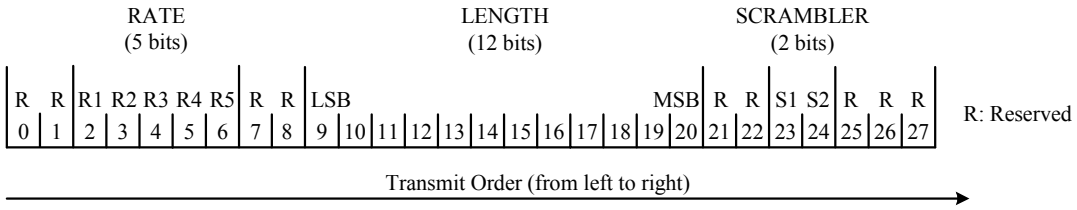

Figure 2.7: PHY header bit assignment of the MB OFDM system

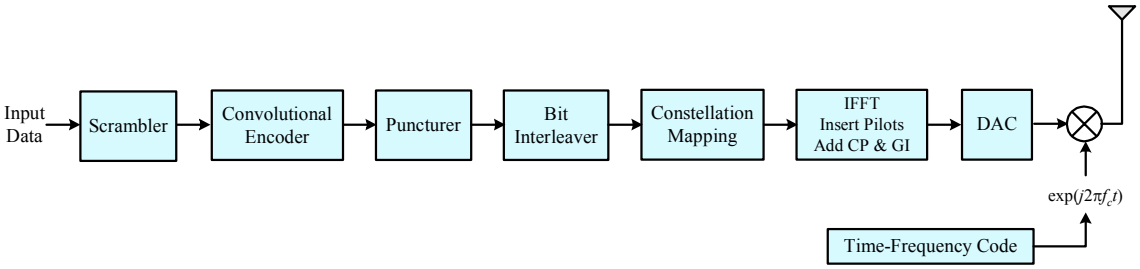

Figure 2.8: The transmitter architecture of MB OFDM system

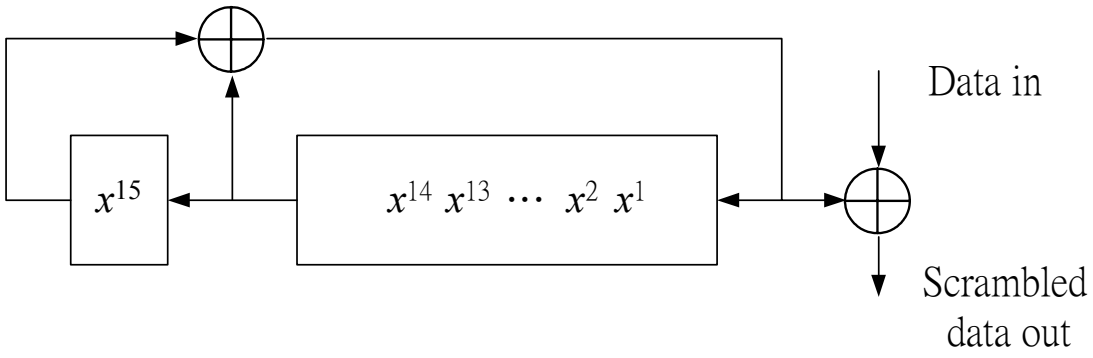

Figure 2.9: Scrambler/descrambler schematic diagram in MB OFDM system

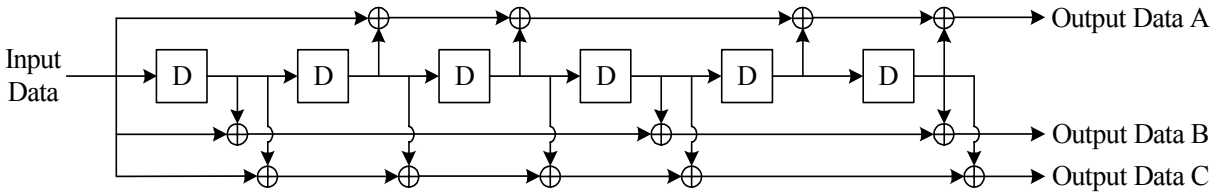

Figure 2.10: Convolutional encoder: rate R = 1/3, constraint length K = 7

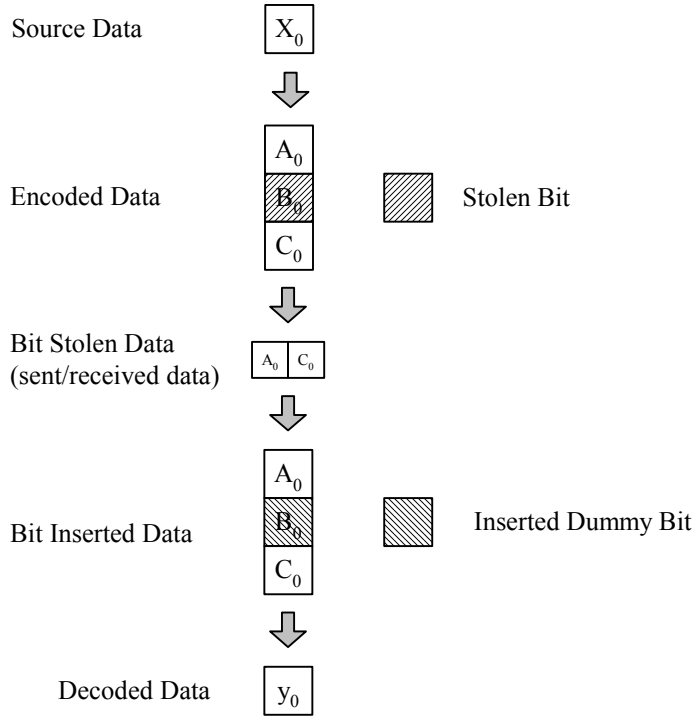

Figure 2.11: An example of the bit-stealing and bit-insertion procedure (R=1/2)

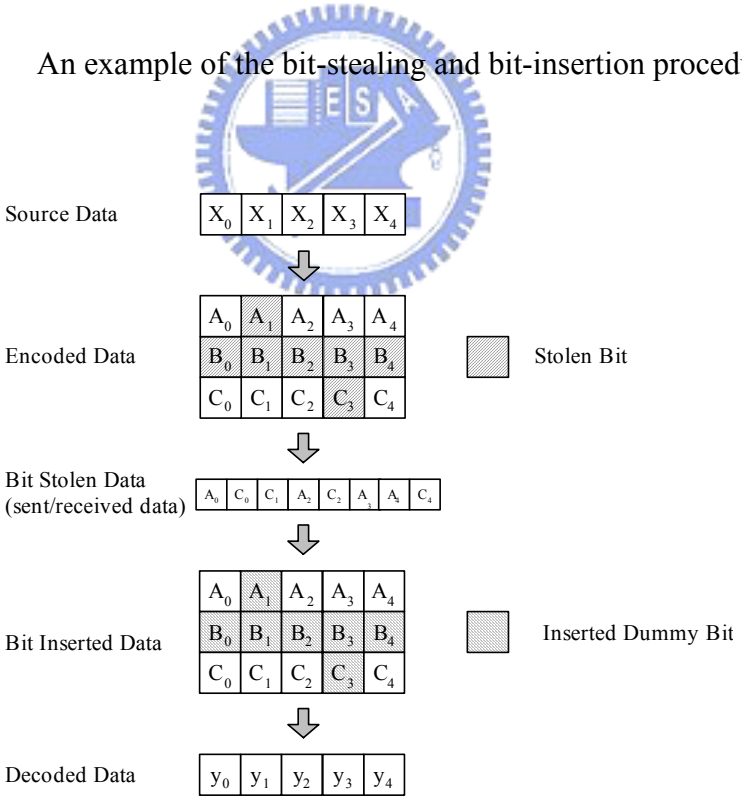

Figure 2.12: An example of the bit-stealing and bit-insertion procedure (R=5/8)

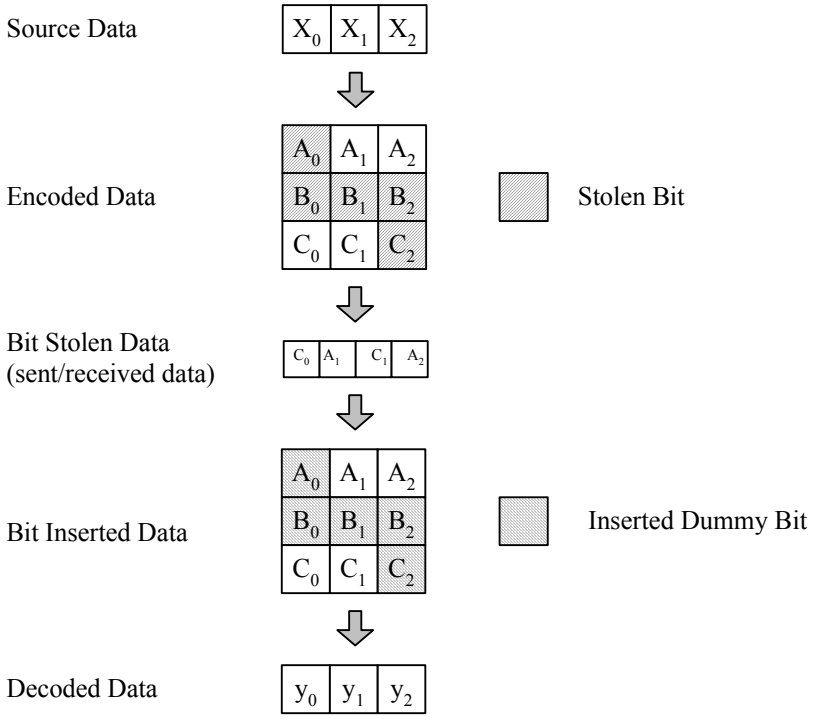

Figure 2.13: An example of the bit-stealing and bit-insertion procedure (R=3/4)

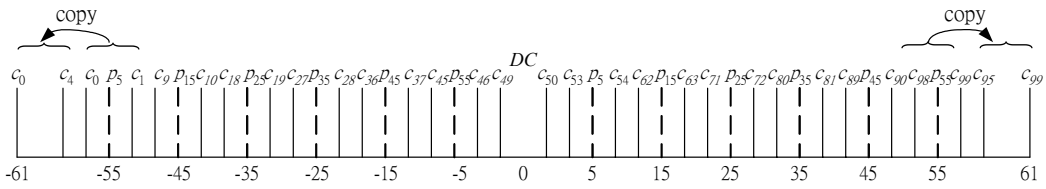

Figure 2.14: Guard subcarrier creation based on edge subcarriers of the MB OFDM symbol

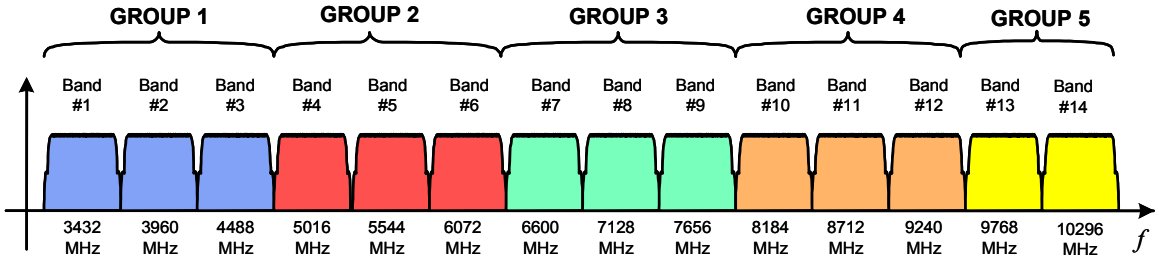

Figure 2.15: Frequency of operation for the MB OFDM system

Table 2.1: Rate-dependent parameters of PHY header for the MB OFDM system

Rate (Mb/s)	R1 – R5
53.3	00000
55	01000
80	00001
106.67	00010
110	01010
160	00011
200	00100
320	00101
400	00110
480	00111
Reserved	01001, 01011–11111

Table 2.2: The data rate dependent modulation parameters of the MB OFDM system

Data Rate (Mb/s)	Modulation	Coding rate (R)	Conjugate Symmetric Input to IFFT	Time Spreading Factor	Overall Spreading Gain	Coded bits per OFDM symbol (N_{CBPS})
53.3	QPSK	1/3	Yes	2	4	100
80	QPSK	½	Yes	2	4	100
106.7	QPSK	1/3	No	2	2	200
160	QPSK	½	No	2	2	200
200	QPSK	5/8	No	2	2	200
320	QPSK	½	No	1	1	200
400	QPSK	5/8	No	1	1	200
480	QPSK	¾	No	1	1	200

Table 2.3: Scrambler seed selection of PHY header for the MB OFDM system

Seed identifier (b_1, b_0)	Seed value (x_{14} … x_0)
0,0	0011 1111 1111 111
0,1	0111 1111 1111 111
1,0	1011 1111 1111 111
1,1	1111 1111 1111 111

Table 2.4: Modulation-dependent normalization factor K_{MOD} for OFDM symbols

Modulation	K_{MOD}
QPSK	$1/\sqrt{2}$

Table 2.5: QPSK encoding table for OFDM symbols

Input bit (b_0 b_1)	I-out	Q-out
00	-1	-1
01	-1	1
10	1	-1
11	1	1

Table 2.6: Time frequency interleaving codes and associated preamble patterns for the MB OFDM system

TFC Number	Preamble Pattern number	Cover Sequence number	Length 6 Time Frequency Code					
1	1	1	1	2	3	1	2	3
2	2	1	1	3	2	1	3	2
3	3	2	1	1	2	2	3	3
4	4	2	1	1	3	3	2	2
5	1	2	1	2	1	2	1	2
6	2	2	1	1	1	2	2	2

Chapter 3

Intercarrier Interference (ICI) Compensation in IEEE 802.15.3a Multi-band OFDM System

Due to its wide bandwidth, a new UWB channel model is developed by the IEEE 802.15.3a standard and is described in this chapter. For highly dispersive channels, some conventional OFDM receiver algorithms are not suitable anymore. In this chapter, the indoor UWB channel model and conventional synchronization techniques for the IEEE 802.15.3a MB OFDM system will be introduced first. Then, the zero padded prefix (ZPP) OFDM system will be introduced in the following section. In addition, the phenomenon and the equalization scheme for long delay spread channels will be described. Finally, the performance simulations are shown in Section 3.5.

3.1 Indoor UWB Channel Model

All wireless systems must be able to deal with the challenges of operating over a multipath propagation channel, where objects in the environment can cause

multiple reflections to arrive at the receiver. The different multipath components (MPCs) are characterized by different delays and attenuations. The correct modeling of the parameters describing the MPCs is the art of channel modeling [15][16].

For narrow-band systems, these reflections will not be resolvable by the receiver when the narrow-band system bandwidth is less than the coherence bandwidth of the channel. When there are a large number of arriving paths at the receiver within its resolution time, the central limit theorem is commonly invoked in order to model the received envelope as a Rayleigh random variable. However, in UWB systems, the large bandwidth of UWB waveforms significantly increases the ability of the RX to resolve the different reflections in the channel. This large bandwidth can give rise to two effects. First, the number of reflections arriving at the receiver within the period of a very short impulse becomes smaller as the duration of the impulse gets shorter and shorter, so the central limit theorem used to justify a Rayleigh distribution for the receiver signal envelop is no longer applicable. Second, the multipath components may be resolved on a very fine time scale (proportional to the inverse of the signal bandwidth), and the time of arrival of the multipath components may not be continuous. This phenomenon could explain the "clustering" of multipath components. For a realistic performance assessment, a UWB channel model like the 802.15.3a standard model has to include all those effects.

Three main indoor channel models were considered: the tap-delay line Rayleigh fading model [17], the Saleh-Valenzuela (S-V) model [18], and the Δ-K model described in [19]. These models use a statistical process to model the discrete arrivals of the multipath components. However, the S–V model is unique in its approach of modeling arrivals in clusters, as well as rays within a cluster. This extra degree of freedom yielded better matching of the model to the channel characteristics gathered from measurement data. As a result, the IEEE 802.15.3a standards body selected the

S–V model, which then needed to be properly parameterized in order to accurately reflect the unique characteristics of the measurements.

3.1.1 Saleh-Valenzuela Model

The S-V model models the multipath of an indoor environment for wideband channels. In order to capture this effect, The S-V model distinguishes between "cluster arrival rates" and "ray arrival rates," where the first cluster starts by definition at time t = 0, and the rays within the cluster arrive with a rate, given by a Poisson process with a start time relative to the cluster arrival time.

Though, the original S-V model has the characteristic that the amplitude statistics sufficiently match the Rayleigh distribution, the power of which is controlled by the cluster and ray decay factors. However, in UWB channels the amplitudes do not follow a Rayleigh distribution. Rather, either a lognormal or Nakagami distribution can fit the data equally well, which has been verified using Kolmogorov-Smirnov testing with a 1 percent significance level. According to these results, the S-V model was modified for the IEEE model by prescribing a lognormal amplitude distribution. The model also includes a shadowing term to account for total received multipath energy variation that result from blockage of the line-of-sight path. The impulse response of multipath model is described as

$$h_i(t) = X_i \sum_{l=0}^{L} \sum_{k=0}^{K} \alpha_{k,l}^{i} \delta\left(t - T_l^i - \tau_{k,l}^i\right) \tag{3.1}$$

where $\alpha_{k,l}^{i}$ are the multipath gain coefficient, T_l^i is the delay of the lth cluster, $\tau_{k,l}^i$ is the delay of the kth multipath component relative to the lth cluster arrival time T_l^i, X_i represents the lognormal shadowing, and i refers to the ith realization.

By definition, we have $\tau_{0,l} = 0$. The distribution of cluster arrival time and the ray arrival time are given by the independent interarrival exponential probability

density function

$$p\left(T_l \mid T_{l-1}\right) = \Lambda \exp\left[-\Lambda\left(T_l - T_{l-1}\right)\right], \quad l > 0 \tag{3.2}$$

$$p\left(\tau_{k,l} \mid \tau_{(k-1),l}\right) = \lambda \exp\left[-\lambda\left(\tau_{k,l} - \tau_{(k-1),l}\right)\right], \quad k > 0 \tag{3.3}$$

where Λ is the cluster arrival rate, and λ is the ray arrival rate, i.e., the arrival rate of a path within each cluster. The channel coefficients are defined as follows:

$$\alpha_{k,l} = p_{k,l}\xi_l\beta_{k,l} \tag{3.4}$$

where ξ_l reflects the fading associated with the *l*th cluster and $\beta_{k,l}$ corresponds to the fading associated with the *k*th ray of the *l*th cluster, the small-scale amplitude statistics were modeled as a lognormal distribution rather than the Rayleigh distribution, whichwas used in the original S–V model, which is reflected in the following equations

$$20\log 10\left(\xi_l\beta_{k,l}\right) \propto \text{Normal}\left(\mu_{k,l}, \sigma_1^2 + \sigma_2^2\right) \text{ or } \left|\xi_l\beta_{k,l}\right| = 10^{\left(\mu_{k,l}+n_1+n_2\right)/20} \tag{3.5}$$

where $n_1 \propto \text{Normal}\left(0, \sigma_1^2\right)$ and $n_2 \propto \text{Normal}\left(0, \sigma_2^2\right)$ are independent and correspond to the fading on each cluster and ray, respectively. σ_1 is standard deviation of cluster lognormal fading term (dB). σ_2 is standard deviation of ray lognormal fading term (dB).

The behavior of the averaged power delay profile is

$$E\left[\left|\xi_l\beta_{k,l}\right|^2\right] = \Omega_0 e^{-T_l/\Gamma} e^{-\tau_{k,l}/\gamma} \tag{3.6}$$

where T_l is the excess delay of bin *l* and Ω_0 is the mean energy of the first path of the first cluster, and $p_{k,l}$ is equiprobable ±1 to account for signal inversion due to reflections. The $\mu_{k,l}$ is given by

$$\mu_{k,l} = \frac{10\ln(\Omega_0) - 10T_l/\Gamma - 10\tau_{k,l}/\gamma}{\ln(10)} - \frac{(\sigma_1^2 + \sigma_2^2)\ln(10)}{20} \tag{3.7}$$

Then, the large-scale fading coefficient is also modeled as a log-normal random

variable in order to capture shadowing effects in the channel. the lognormal shadowing of the total multipath energy is captured by the term, X_i, the total energy contained in the terms $\alpha_{k,l}^{i}$ is normalized to unity for each realization. This shadowing term is characterized by the following

$$20\log 10(X_i) \propto \text{Normal}(0, \sigma_x^2) \tag{3.8}$$

Note that, a complex tap model was not adopted here. The complex baseband model is a natural fit for narrowband systems to capture channel behavior independently of carrier frequency, but this motivation does not work for UWB systems where a real-valued simulation at RF may be more natural. Figure 3.1 illustrates the equivalent model for simulation of passband system in terms of complex baseband system. Therefore the real-valued passband multipath channel response is simplified as follow

$$h(t) = \sum_{i=1}^{P} \alpha_i \delta\left(t - \tau_i\right) \tag{3.9}$$

where α_i is the real-values channel coefficient. The equivalent baseband multipath channel response is described by

$$\tilde{h}(t) = \sum_{i=1}^{P} \alpha_i e^{-j2\pi f_c \tau_i} \delta\left(t - \tau_i\right) = \sum_{i}^{P} \tilde{\alpha}_i \delta\left(t - \tau_i\right) \tag{3.10}$$

The UWB model parameters were designed to fit measurement results, and Table 3.1 provides the results of this fit for four kinds different channel scenarios (LOS refers to line of sight, NLOS to non-LOS).

(1). CM1 is based on LOS (0 – 4 m) channel measurements.

(2). CM2 is based on NLOS (0 – 4 m) channel measurements.

(3). CM3 is based on NLOS (4 – 10 m) channel measurements.

(4). CM4 is generated to fit a 25 ns RMS delay spread to represent an extreme

NLOS multipath channel.

As shown in Figures 3.2 and 3.3, along with the channel measurement characteristics listed in Table 3.1, highlight characteristics of the multipath channel that are important to discuss. The multipath spanning several nanoseconds in time result in ISI when UWB pulses is closely spaced in time. However, there are many way to mitigate the interference through proper waveform design as well as signal processing and equalization algorithms. Besides, the extremely wide bandwidth of a transmitted pulse results in the ability to individually resolve several multipath components.

3.2 Receiver Architecture

One of the major drawbacks of OFDM systems is its high sensitivity to synchronization errors. Without accurate synchronization algorithm, it is not possible to reliably receive the transmitted data. In a MB OFDM system, the preamble is used for the sake of synchronizing OFDM signals. In the following section we will introduce the receiver architecture of the MB OFDM system, as shown in Figures 3.4, in detail [20].

3.2.1 Synchronization

Synchronization is a fundamental assignment for any communication system and should be done before the other work like channel estimation and data demodulation. Synchronization has two parts: timing synchronization and frequency synchronization

Packet Detection

Packet detection is the task of finding an approximate estimate of the start of the preamble of an incoming data packet as best it can. Because it is the first synchronization algorithm, the rest of the synchronization process is dependent on good packet detection performed. Fortunately, the preamble of the MB OFDM system has been designed to help the detection of the start edge of the packet. The cross-correlation method takes advantage of the periodicity of the synchronization symbols at the start of the preamble. As shown in Figure 3.5, the matched filter with the coefficient of the preamble sequence is proposed to correlate the received symbols. The preamble sequence is pre-assigned by the piconet channel of MAC layer. When some threshold of correlation is exceeded by the output power of the post-matched filter, the receiver will declare a packet detection. The commonly used value of the threshold is more than 250.

Symbol Timing Estimation

When the start of the preamble of an incoming data packet has been captured, the following job is symbol timing estimation finding the precise moment of when individual OFDM symbols start and end. The result of symbol timing estimation will circumscribe the DFT window, and the DFT result is then used to demodulate the subcarriers of the symbol. MB OFDM receiver has knowledge of the preamble available to them, which enables the receiver to use simple cross-correlation based symbol timing algorithm. According to an estimate of the start edge of the packet provided by packet detector, the symbol timing estimation algorithm improves the estimate to sample level precision, as shown in Figure 3.6. The refinement is performed by calculating the cross-correlation of the received signal r_n and a known reference s_k . The known reference s_k can be the end of the

synchronization symbols or the start of the channel estimation symbols. Equation 3.11 shows how to calculate the cross-correlation. The value of *n* that corresponds to maximum absolute value of the cross-correlation is the symbol timing estimate.

$$\hat{t}_s = \arg\max_n \left| \sum_{k=0}^{L-1} r_{n+k} s_k^* \right|^2 \tag{3.11}$$

where the length L of the cross-correlation determines the performance of the algorithm. Larger value improves performance, but also increases the amount of computation required.

Frequency Synchronization

OFDM is highly sensitive to carrier frequency offset. It results in two main phenomena: reduction of amplitude of the desired subcarrier and ICI caused by nearby subcarriers. The first phenomena results from that the desired subcarrier is not sampled at the peak of the sinc function. The reason of second phenomena is that adjacent subcarriers are not sampled at the zero-crossings of their sinc function. The degradation in dB can be approximated by

$$SNR_{Loss} = \frac{10}{3\ln 10}\left(\pi T f_\Delta\right)^2 \frac{E_s}{N_0} \text{dB} \tag{3.12}$$

where f_Δ is the frequency error as a fraction of the subcarrier spacing and T is the sampling period.

Frequency Offset Tracking

The data-aided algorithm is appropriate for the MB OFDM system. The preamble allows the receiver to use efficient maximum likelihood algorithm to estimate and correct for the frequency offset, before the actual information portion of the packet starts.

We introduce the algorithm that operates on the received time domain signal as

shown in Figure 3.7. First, the transmitted passband signal is

$$y_n = s_n e^{j2\pi f_{tx} nT_s} \tag{3.13}$$

where s_n is the baseband signal and f_{tx} is the transmitter carrier frequency. The received signal r_n is

$$\begin{aligned} r_n &= s_n e^{j2\pi f_{tx} nT_s} e^{-j2\pi f_{rx} nT_s} \\ &= s_n e^{j2\pi\left(f_{tx} - f_{rx}\right)nT_s} \\ &= s_n e^{j2\pi f_\Delta nT_s} \end{aligned} \tag{3.14}$$

where f_{rx} is the receiver carrier frequency and $f_\Delta = f_{tx} - f_{rx}$ is the difference between the transmitter and receiver carrier frequencies. Let D be the delay between the identical samples of the two repeated symbols. Then, the frequency offset estimator is developed as follows, starting with an intermediate variable z

$$\begin{aligned} z &= \sum_{n=0}^{L-1} r_n r_{n+D}^* \\ &= \sum_{n=0}^{L-1} s_n e^{j2\pi f_\Delta nT_s} \left(s_{n+D} e^{j2\pi f_\Delta (n+D)T_s}\right)^* \\ &= \sum_{n=0}^{L-1} s_n s_{n+D}^* e^{j2\pi f_\Delta nT_s} e^{-j2\pi f_\Delta (n+D)T_s} \\ &= e^{-j2\pi f_\Delta DT_s} \sum_{n=0}^{L-1} |s_n|^2 \end{aligned} \tag{3.15}$$

We observe that an angle of z is proportional to the frequency offset, and the frequency offset estimator is obtained by

$$\hat{f}_\Delta = -\frac{1}{2\pi DT_s} \angle z \tag{3.16}$$

where the $\angle z$ operator takes the angle of its argument

Carrier Phase Tracking

There is always some residual frequency error, because the frequency estimation is not accurate. The residual frequency offset results in constellation rotation. This is the reason why the receiver has to track the carrier phase after data symbols are received.

Data-aided tracking of the carrier phase is simple method for MB OFDM system. There are twelve predefined subcarriers among the transmitted data. These special subcarriers are referred to as pilot subcarriers. The receiver can exactly track the carrier phase with these pilots, symbol by symbol. After the DFT of the *n*th received symbol, the pilot subcarriers $R_{n,k}$ are equal to the product of channel frequency response H_k and the known pilot symbols $P_{n,k}$, rotated by the residual frequency error.

$$R_{n,k} = H_k P_{n,k} e^{j2\pi n f_\Delta} \tag{3.17}$$

Assuming as estimate $\tilde{H}_k$ of the channel frequency response is available, the phase estimate is

$$\tilde{\Phi}_n = \angle\left[\sum_{k=1}^{N_p} R_{n,k}\left(\tilde{H}_k P_{n,k}\right)^*\right] = \angle\left[\sum_{k=1}^{N_p} H_k P_{n,k} e^{j2\pi n f_\Delta}\left(\tilde{H}_k P_{n,k}\right)^*\right] \tag{3.18}$$

If the channel estimate is perfectly accurate, we get the estimator

$$\tilde{\Phi}_n = \angle\left[\sum_{k=1}^{N_p} \left|H_k\right|^2 \left|P_{n,k}\right|^2 e^{j2\pi n f_\Delta}\right] = \angle\left[e^{j2\pi n f_\Delta} \sum_{k=1}^{N_p} \left|H_k\right|^2\right] \tag{3.19}$$

There is no the phase ambiguity problem, because the pilot data are known at receiver. However, the channel estimation is not perfectly accurate, thus they contribute to the noise in the estimate.

3.2.2 Channel Estimation

In wideband communication systems, under the assumption of a slow fading channel, in which the channel transfer function is stationary within a packet duration, preambles or training sequences can be used to estimate the channel response for the following OFDM data symbols in the same packet. The channel estimation symbols in the preamble facilitate an powerful estimate of the channel frequency response for all the subcarriers. The quality of the channel estimation can be improved by averaging the two channel estimation symbols, because they are entirely identical symbols. the two received channel estimation symbols $R_{1,k}$ and$R_{2,k}$ are a product of the channel estimation symbol X_k and the channel H_k plus additive white Gaussian noise $N_{l,k}$

$$R_{l,k} = H_k X_k + N_{l,k} \quad l = 1,2 \tag{3.20}$$

Thus the channel estimate can be calculated as

$$\begin{aligned} \hat{H}_k &= \frac{1}{2}\left(R_{1,k} + R_{2,k}\right)X_k^* \\ &= \frac{1}{2}\left(H_k X_k + N_{1,k} + H_k X_k + N_{2,k}\right)X_k^* \\ &= H_k \left|X_k\right|^2 + \frac{1}{2}\left(N_{1,k} + N_{2,k}\right)X_k^* \\ &= H_k + \frac{1}{2}\left(N_{1,k} + N_{2,k}\right)X_k^* \end{aligned} \tag{3.21}$$

where the channel estimation data power have been selected to be equal to one. The noise samples $N_{1,k}$ and $N_{2,k}$ are statistically independent, thus the variance of their sum divide by two is a half of the variance of the individual noise samples.

3.3 Zero Padded Prefix (ZPP) OFDM System

Due to the IFFT precoding and the insertion of CP at the transmitter, OFDM entails redundant block transmissions and employs simple equalization of

frequency-selective finite impulse response (FIR) channels. At the receiver, intersymbol interference (ISI) and intercarrier interference (ICI) can be eliminated by discarding the CP. Unless zero, flat fades can be removed by dividing each subchannel's output with the channel transfer function at the corresponding subcarrier. Therefore, most current wireless OFDM-based systems use a CP to eliminate the effect of multipath.

However, the same multipath robustness can be obtained by using a zero padded prefix (ZPP) instead of the CP [21]-[23]. At transmitter, zero symbols are appended after the IFFT-precoded information symbols in each block of the ZPP OFDM transmission. When the number of zero symbols equals the CP length, the ZPP OFDM system can provide the same multipath robustness as the CP OFDM system. What we have to modify at the receiver is to collect additional samples corresponding to the length of the prefix and to use the overlap-and-add method to obtain the circular convolution structure.

Due to ZPP, the "time domain" received signal of OFDM symbol can be expressed as

$$\mathbf{y} = \mathbf{H}\mathbf{x} + \boldsymbol{\eta}$$

$$\underbrace{\begin{bmatrix} y_0 \\ \vdots \\ y_{N_c-1} \\ \vdots \\ y_{N_{zp}+N_c-1} \end{bmatrix}}_{\mathbf{y}} = \underbrace{\begin{bmatrix} h_0 & 0 & \cdots & \cdots & \cdots & 0 \\ h_1 & h_0 & 0 & \ddots & \ddots & 0 \\ h_2 & h_1 & h_0 & 0 & \cdots & 0 \\ \vdots & \ddots & \ddots & \ddots & \ddots & \vdots \\ h_L & \ddots & \ddots & \ddots & \ddots & \vdots \\ 0 & h_L & \ddots & \ddots & \ddots & 0 \\ \vdots & \ddots & h_L & \ddots & \ddots & \vdots \\ 0 & \cdots & 0 & h_L & \cdots & h_0 \end{bmatrix}}_{\mathbf{H}} \underbrace{\begin{bmatrix} x_0 \\ x_1 \\ \vdots \\ x_{N_c-1} \\ 0 \\ \vdots \\ 0 \end{bmatrix}}_{\mathbf{x}} + \underbrace{\begin{bmatrix} \eta_0 \\ \vdots \\ \eta_{N_c-1} \\ \vdots \\ \eta_{N_{zp}+N_c-1} \end{bmatrix}}_{\eta} \tag{3.22}$$

where N_c is number of subcarrier, N_{zp} is the length of ZPP and L is the length of channel impulse response. Then collect y_{N_c} to $y_{N_{zp}+N_c-1}$ samples corresponding to the length of the ZPP and use an overlap-and-add method, the received signal of

OFDM symbol can be expressed as

$$\begin{bmatrix} y_0 \\ \vdots \\ y_{N_c-1} \end{bmatrix} = \begin{bmatrix} y_0 + y_{N_c} \\ y_1 + y_{N_c+1} \\ \vdots \\ y_{N_{ZP}-1} + y_{N_c+N_{ZP}-1} \\ y_{N_{ZP}} \\ \vdots \\ y_{N_c-1} \end{bmatrix} = \begin{bmatrix} h_0 & 0 & \cdots & h_L & h_{L-1} & \cdots & h_1 \\ h_1 & h_0 & 0_1 & \cdots & h_L & \ddots & h_2 \\ \vdots & h_1 & \ddots & \ddots & \ddots & \ddots & \vdots \\ h_L & \cdots & \ddots & h_0 & 0 & \cdots & h_L \\ 0 & h_L & \cdots & \ddots & h_0 & \cdots & 0 \\ \vdots & \ddots & \ddots & \ddots & \ddots & \ddots & \vdots \\ 0 & \cdots & 0 & h_L & \cdots & h_1 & h_0 \end{bmatrix} \begin{bmatrix} x_0 \\ \vdots \\ x_{N_c-1} \end{bmatrix} + \begin{bmatrix} \eta_0' \\ \vdots \\ \eta_{N_c-1}' \end{bmatrix} \quad (3.23)$$

From Equation 3.23, we see that the ZPP OFDM system with overlap-and-add method is equivalent to the CP OFDM system, because they have the same overall transceiver transfer function. It is, thus, not surprising that they has identical property: complexity, spectral efficiency, and multipath robustness.

Though, there are many the same characterizes between two systems. They still have some differences. The most important advantage of using a ZPP is that power backoff at the transmitter can be avoided. When a CP is used, the transmitted signal will have the structure resulting from CP. This correlation in the transmitted signal induces ripples in the average PSD. Because the FCC limits the PSD of UWB, any ripples in the PSD will lead to power back off at the transmitter. In fact, the amount of power backoff to conform to the restriction of FCC is equal to the peak-to-average ratio of the PSD. For a MB OFDM system, this power backoff will arrive at 1.5 dB, which would result in a lower overall range for the system. When the ZPP instead of the CP, the ripples in the PSD can be reduced to zero with enough averaging. The transmitted signal does not have any structure; because it is completely random. Figures 3.8 and 3.9 indicate the ripples in the PSD for a MB OFDM system that uses a CP and ZPP. From two figures, they show that the ZPP will result in a PSD with zero ripples and a zero power backoff at the transmitter. This implies that the system will achieve the maximum range possible. In addition to the ripples in the PSD, the CP OFDM system has to spend the energy for CP, but the ZPP OFDM system does

not. However, the receiver will pick up larger noise because the ZPP OFDM system uses an overlap-and-add method to obtain the circular convolution property. This will lead to the noise enhancement as shown in Figure 3.10.

3.3.1 ZPP OFDM System Model for Long Delay Spread Channel

Although, the channel impairment can be overcome by introducing ZPP and completely eliminated by the simple one-tap equalizer in case the length of ZPP is longer than that of the channel impulse response. However, the large bandwidth of the MB OFDM waveform (528 MHz) significantly increases the ability of the receiver to resolve the different reflections in the channel and shortens the OFDM symbol duration. These results make the length of the channel impulse response may be longer than the length of ZPP, especially for CM4 channel. Consequently, the ISI and ICI will be induced and result in performance degradation [24]-[30].

Analysis of ISI and ICI

Figure 3.11 describes the ISI and ICI are introduced in the multipath channels. The ISI results from the portion of the previous symbol included in the current FFT window. The ICI is caused by the current symbol loss due to the long delayed paths exceed the prefix interval. The influence of ISI and ICI can be analyzed based on the above observation. The received signal can be written in the frequency domain as follows

$$\mathbf{Y}_n = \mathbf{FHF}^*\mathbf{X}_n - \mathbf{FH}_{ICI}\mathbf{F}^*\mathbf{X}_n + \mathbf{FH}_{ISI}\mathbf{F}^*\mathbf{X}_{n-1} + \mathbf{N}_n \tag{3.24}$$

where **F** is a FFT matrix, then **H,** $\mathbf{H}_{ICI}$ and $\mathbf{H}_{ISI}$ are given as

$$\mathbf{H}=\begin{bmatrix} h_0 & 0 & \cdots & h_L & \cdots & \cdots & h_2 & h_1 \\ h_1 & h_0 & \cdots & 0 & h_L & \cdots & h_3 & h_2 \\ \vdots & \vdots & & \vdots & & & \vdots & \vdots \\ h_{L-1} & h_{L-2} & & h_0 & 0 & & & h_L \\ h_L & h_{L-1} & \ddots & h_1 & h_0 & \ddots & & 0 \\ \vdots & & \ddots & & \ddots & & \ddots & \vdots \\ & \cdots & & h_L & h_{L-1} & \cdots & h_1 & h_0 \end{bmatrix} \tag{3.25}$$

$$\mathbf{H}_{ICI}=\begin{bmatrix} 0_1 & 0_1 & \cdots & 0_1 & \cdots & 0_1 \\ \vdots & \ddots & & \ddots & \ddots & \vdots \\ 0_{ZP} & 0_{ZP} & \ddots & 0_{ZP} & & 0_{ZP} \\ 0 & \cdots & h_L & h_{L-1} & \cdots & h_{N_{ZP}+1} \\ 0 & \ddots & \ddots & h_L & \ddots & h_{N_{ZP}+2} \\ \vdots & & \ddots & & \ddots & \vdots \\ 0 & & \ddots & & & h_L \\ \vdots & & & & & \vdots \\ 0 & \cdots & 0 & 0 & \cdots & 0 \end{bmatrix} \tag{3.26}$$

$$\mathbf{H}_{ISI}=\begin{bmatrix} 0 & \cdots & h_L & h_{L-1} & \cdots & h_{N_{ZP}+1} \\ 0 & \cdots & 0 & h_L & \ddots & h_{N_{ZP}+2} \\ \vdots & \cdots & \vdots & & & \\ 0 & \cdots & 0 & 0 & \ddots & h_L \\ \vdots & \cdots & \vdots & & & \\ 0 & \cdots & 0 & 0 & \ddots & 0 \end{bmatrix} \tag{3.27}$$

where N_{zp} is the length of ZPP, and L is the length of the channel impulse response. The shapes of $\mathbf{H}_{ICI}$ and $\mathbf{H}_{ISI}$ are shown in Figure 3.12. ISI is caused by the non-zero components of $\mathbf{H}_{ISI}$, and the ICI results from an element loss that distorts a cyclic shift formation in $\mathbf{H}_{ICI}$. According to the two relationships, the performance degradation due to ISI and ICI can be evaluated.

At first, signal-to-interference ratio (SIR) is calculated as a function of the amount of ISI and ICI. Assuming without loss of generality the ideal signal power is that of the received symbol when the length of the ZPP is longer than the channel

impulse response. Besides, according to the Specification of MB OFDM system, there are 128 subcarriers in one OFDM symbol. The ideal OFDM symbol power is defined as

$$P_{sig} = E\left\{\sum_{j=0}^{N-1}\left|\sum_{i=0}^{L-1} x(\mathrm{MOD}(j-i,N))h(i)\right|^2\right\} = 128\sum_{i=0}^{L-1}\left|h(i)\right|^2 \tag{3.28}$$

where E{.} is an expectation function and *x*(MOD(*j*-*i*,*N*)) is the transmitted signal of MOD(*j*-*i*,*N*)th subcarrier. Then, the E{x(n)} is zero-mean with unit variance and uncorrelated because the data and channel are independent. From Figure 3.12, power of ISI and ICI are given as

$$P_{ISI} = P_{ICI} = \sum_{i=1}^{L-N_{ZP}-1} i\left|h(N_{ZP}+i)\right|^2 \tag{3.29}$$

The *SIR* is

$$SIR = \frac{P_{sig}}{P_{ICI}+P_{ISI}} = \frac{128\sum_{i=0}^{L-1}\left|h(i)\right|^2}{2\times\sum_{i=1}^{L-N_{ZP}-1} i\left|h(N_{ZP}+i)\right|^2} \tag{3.30}$$

However, the MB OFDM system uses the modulation technique and the multibanding approach dividing the spectrum into several sub-bands. The transmitted OFDM symbols are conveyed across all sub-bands. So the received OFDM symbols suffer only the impact of ICI.

3.4 ICI Compensation for IEEE 802.15.3a MB OFDM System

Several different schemes have existed to overcome the performance degradation resulting from long delay spread channels. The simplest method is to extend the length of ZPP. As long as the ZPP is extended longer than channel impulse

response, ICI can be avoided. However, the major drawback of this scheme is to decrease the system efficiency. For example, 32-sample ZPP can be substituted with 64-sample ZPP to eliminate the ICI. In the MB OFDM system the size of FFT is 128, the overhead increases from 25% to 50% and the throughput becomes lower. Therefore the system targeting for the high efficiency cannot adopt the approach.

3.4.1 ICI Compensation Using MRC

In the MB OFDM system, the time-domain spreading operation is performed for the 200 Mbps and lower than 200 Mbps data rate modes. Two identical OFDM symbols are transmitted over different sub-bands in order to obtain frequency diversity. The replicas of the transmitted signals are provided to the receiver in the form of redundancy in the frequency domain.

Scenario considered herein involves a time-domain spreading system. After FFT processing, the received signal in the frequency domain can be expressed as

$$\mathbf{Y}^i = \mathbf{FHF}^*\mathbf{X}^i - \mathbf{FH}_{ICI}\mathbf{F}^*\mathbf{X}^i + \mathbf{N}^i \quad \forall i = 1,2 \tag{3.31}$$

where $\mathbf{Y}^i = \left[Y_0^i \;\; Y_1^i \cdots Y_{N_c-1}^i\right]^T$, $\mathbf{X}^i = \left[X_0^i \;\; X_1^i \cdots X_{N_c-1}^i\right]^T$, and $\mathbf{N}^i = \left[N_0^i \;\; N_1^i \cdots N_{N_c-1}^i\right]^T$ are the receiver signal, the transmitted signal and the add white gaussian noise in the frequency domain, respectively. As shown in Figure 3.13, the magnitude of ICI components is distributed randomly, and the X_k is QPSK signal, E$\{X\}$ is zero-mean with unit variance and uncorrelated. Then, the ICI components are considered as a Normal distribution with zero mean and σ_{ICI}^2 variance.

The output of MRC is given by

$$\tilde{Y}_{k,MRC} = \left[H_k^1\right]^* Y_k^1 + \left[H_k^2\right]^* Y_k^2 \tag{3.32}$$

where k is the subcarrier index. Thus, we can calculate mean and variance of $\tilde{Y}_{k,MRC}$ as follows

$$\mu_{\tilde{Y}_{k,MRC}} = a_{k,MRC} X_k \tag{3.33}$$

$$\sigma^2_{\tilde{Y}_{k,MRC}} = N_c a_{k,MRC} \left(\sigma^2_{ICI} + \sigma^2_n\right) \tag{3.34}$$

where $a_{k,MRC} = \frac{1}{N_c}\left[\left|H_k^1\right|^2 + \left|H_k^2\right|^2\right]$. Finally, BER for MRC can be obtained from Equation 3.35. It shows that diversity gain gives a direct solution for joint suppression of ICI and noise.

$$P_{e,MRC} = \frac{1}{N_c}\sum_{k=0}^{N_c-1} Q\left[\frac{a_{k,MRC}}{\sigma_{Y_{k,MRC}}}\right] = \frac{1}{N_c}\sum_{k=0}^{N_c-1} Q\left[\frac{1}{\sqrt{\frac{\sigma^2_{ICI}+\sigma^2_n}{N_c a_{k,MRC}}}}\right] \tag{3.35}$$

3.4.2 ICI Compensation Using MMSE Equalizer

Unfortunately, there is no time-domain or frequency-domain spreading operation for 320 Mbps and higher than 320 Mbps data rate mode. Consequently, the receiver with higher data rate mode cannot suppress the ICI by MRC. The minimum mean-square error (MMSE) equalizer is the most common method. Because the symbols have variance $\sigma_s^2 = 1$, the MMSE equalizer for an additive white gaussian noise of variance σ_n^2 is given as

$$\mathbf{G}_{MMSE} = \mathbf{F}\mathbf{H}_0^H \left(\mathbf{H}_0\mathbf{H}_0^H + \sigma_n^2\mathbf{I}\right)^{-1} \tag{3.36}$$

where $\mathbf{H}_0 = \mathbf{H} - \mathbf{H}_{ICI}$. Note that $\mathbf{G}_{MMSE}$ require the inversion of $N_c \times N_c$ matrix which cannot be precomputed since the matrix to be inverted depends on the channel. Hence, the MMSE equalizer incurs an extra implementation cost relative to the FFT-based ZPP OFDM receiver.

3.4.3 ICI Compensation Using Decision-Aided ICI Canceller

Because the matrix inverse computation is too complex for the MB OFDM system, we propose a decision-aided ICI canceller (DAIC) to suppress the impact of ICI, as shown in Figure 3.14. The DAIC is an iterative technique which mitigates the influence of ICI by reconstructing ICI components and eliminating it from received signals. The DAIC is explained as follow:

1) After FFT processing, the received signal **Y** is stored in the memory, and the initial estimate of the transmitted symbol **X** is obtained as

$$X_k = Y_k / H_k, \quad 0 \le k \le N_c - 1 \tag{3.37}$$

where $\mathbf{X} = [X_0, X_1, ..., X_{N_c-1}]^T$, and the ICI components can be reconstruct by the initial estimate.

2) Calculate the ICI components by $\mathbf{H}_{ICI}$ and $\mathbf{X}$. Then, the temporal estimated symbol in the frequency domain is determined by

$$\begin{aligned} \mathbf{X}^{I+1} &= \mathrm{conj}\left\{\mathbf{H}_f\right\}\left(\mathbf{Y} + \mathbf{F}\mathbf{H}_{ICI}\mathbf{F}^*\mathbf{X}^I\right) \\ &= \mathrm{conj}\left\{\mathbf{H}_f\right\}\left(\mathbf{F}\mathbf{H}\mathbf{F}^*\mathbf{X} - \mathbf{F}\mathbf{H}_{ICI}\mathbf{F}^*(\mathbf{X} - \mathbf{X}^I)\right) \end{aligned} \tag{3.38}$$

where $\mathbf{H}_f = [H_0, H_1, ..., H_{N_c-1}]^T$ is the frequency response of the channel, and I represents an iteration number with an initial value of $I = 0$, and $\mathbf{X}^0 = \mathbf{X}$

3) Due to the subcarrier modulation is QPSK, the temporal estimated symbol can be determined by

$$\mathbf{X}^{I+1} = \frac{1}{\sqrt{2}}\mathrm{sgn}\left\{\mathbf{real}(\mathbf{X}^{I+1})\right\} + \frac{1}{\sqrt{2}}\mathrm{sgn}\left\{\mathbf{imag}(\mathbf{X}^{I+1})\right\} \tag{3.39}$$

where sgn represent the “Sign” operator

4) Increase the index number $I \rightarrow I + 1$ and go back to step 2.

In Figure 3.14, the symbol obtained from the output of FFT is used as initial estimated symbol $\mathbf{X}^0$. The estimated ICI component in the first step DAIC is not so

accurate, because initial estimated symbol generally has decision errors. Therefore, temporal estimated symbols $\mathbf{X}^1$, $\mathbf{X}^2$,… for the next iteration are obtained from the output of the previous DAIC repeatedly. The number of errors which the temporal estimated symbol includes is expected to decrease gradually and the ICI components are estimated more accurately every iteration. Consequently, the BER performance can be improved by the DAIC. However, if there are too many errors in initial temporal symbol decisions $\mathbf{X}^0$, the errors which the $\mathbf{X}^0$ includes will induce double interference for next symbol decision $\mathbf{X}^1$. This will result in error propagation.

In above discussion, we assume that the channel state information is available at the receiver and $\mathbf{H}_{ICI}$ can be reconstruction by Equation 3.26. When the temporal estimated symbol has no errors, the ICI component is eliminated completely form the step 2). However, it is impossible to know the channel state information without channel estimation. In the next section we will introduce channel estimation under ICI influence.

3.5 Channel Estimation Using Decision-Aided ICI Canceller

As ICI and noise exist, the correct channel estimates by the preamble are hard to be achieved. Since ICI and noise effects change randomly, the channel estimation using preamble data cannot distortionlessly obtain the channel estimates. Therefore, the receiver fails to successfully restore the transmitted data. The Least Square (LS) channel estimation using training symbols can only divide the variance of noise samples of the training symbols by two. So channel compensation is necessary under the ICI effect. In order to alleviate the ICI effects generated by insufficient ZPP, we also use the decision aided ICI canceller method for ICI compensation. The received

signal in time-domain can be written as

$$\mathbf{y} = \mathbf{H}\mathbf{x} - \mathbf{H}_{ICI}\mathbf{x} + \mathbf{n} \tag{3.40}$$

where $\mathbf{H}$ and $\mathbf{H}_{ICI}$ are shown in Equations 3.25 and 3.26. Because we want to estimate the channel impulse response, the above Equations 3.40 can be rewritten as

$$\mathbf{y} = \mathbf{x}^t\mathbf{h} - \mathbf{x}_{ICI}^t\mathbf{h} + \mathbf{n} \tag{3.41}$$

where $\mathbf{h} = [h_0, h_1, ..., h_{N_c-1}]^T$ is the channel impulse response. Then, $\mathbf{x}$ and $\mathbf{x}_{ICI}$ are given as

$$\mathbf{x}^t = \begin{bmatrix} x_0 & x_{127} & \cdots & x_L & \cdots & \cdots & x_2 & x_1 \\ x_1 & x_0 & x_{127} & \cdots & x_L & \cdots & x_3 & x_2 \\ \vdots & \vdots & & \vdots & & & \vdots & \vdots \\ x_{L-1} & x_{L-2} & & x_0 & x_{127} & & & x_L \\ x_L & x_{L-1} & \ddots & x_1 & x_0 & \ddots & & x_{L+1} \\ \vdots & & \ddots & & \ddots & & \ddots & \vdots \\ & \cdots & & x_L & x_{L-1} & \cdots & x_1 & x_0 \end{bmatrix} \tag{3.42}$$

$$\mathbf{x}_{ICI}^t = \begin{bmatrix} 0 & \overbrace{0 \quad 0}^{N_{zp}} & x_{128-N_{zp}-1} & \cdots & x_3 & x_2 & x_1 \\ \vdots & \vdots \quad 0 & \ddots & x_{128-N_{zp}-1} & \cdots & x_3 & x_2 \\ \vdots & \vdots \quad \vdots & \ddots & & \ddots & \vdots & \vdots \\ \vdots & \vdots \quad \vdots & & & & & x_{128-N_{zp}-1} \\ \vdots & \vdots & \ddots & \ddots & \ddots & & 0 \\ \vdots & \vdots & & & & \ddots & \vdots \\ 0 & \cdots \quad \cdots & 0 & 0 & 0 & 0 & 0 \end{bmatrix} \tag{3.43}$$

Because the preamble x is known at the receiver, we can use the DAIC to estimate the channel impulse response. The method is explained as follow:

1) After FFT processing, the received signal **Y** is stored in the memory, and the initial estimate of the channel frequency response of $\mathbf{H}_f$ is derived as

$$H_k = Y_k / X_k, \quad 0 \le k \le N_c - 1 \tag{3.44}$$

where $\mathbf{H}_f = [H_0, H_1, ..., H_{N_c-1}]^T$, and the ICI components can be reconstruct by the initial estimate.

2) Calculate the ICI components by $\mathbf{x}_{ICI}$ and $\mathbf{H}_f$. Then, temporal estimated channel response $\mathbf{H}_f$ in the frequency domain is determined by

$$\begin{aligned}\mathbf{H}_f^{I+1} &= \left(\mathbf{Y} + \mathbf{F}\mathbf{x}_{ICI}\mathbf{F}^*\mathbf{H}_f^I\right)\Big/\mathbf{X} \\ &= \left(\mathbf{F}\mathbf{x}\mathbf{F}^*\mathbf{H} - \mathbf{F}\mathbf{x}_{ICI}\mathbf{F}^*(\mathbf{H} - \mathbf{H}_f^I)\right)\Big/\mathbf{X}\end{aligned} \tag{3.45}$$

where $\mathbf{x} = [X_0, X_1, ..., X_{N_c-1}]^T$ is the preamble in the frequency domain, and I represents an iteration number with an initial value of $I = 0$, and $\mathbf{H}_f^0 = \mathbf{H}_f$

3) Increase the index number $I \rightarrow I + 1$ and go back to step 2.

Using the DAIC for channel estimation, the receiver can obtain more accurate channel estimates than the LS method. The proposed channel estimation makes the receiver remove ICI and recover the transmitted data accurately.

3.6 Computer Simulations

Computer simulations are conducted to evaluate the performance of the synchronization, channel estimation and proposed ICI compensation methods in the MB OFDM system. In the simulations, the relationship between SNR and E_b/N_0 can be defined as

$$\frac{E_b}{N_0} = \frac{\text{bit power}}{\text{noise power}} = \frac{\frac{E_b}{T_s}}{N_0 \cdot \frac{1}{T_s}} = \frac{\frac{E_s}{T_s M}}{N_0 \cdot B} = SNR \cdot \frac{1}{M}$$

where E_s is the symbol energy, T_s is the symbol duration, B is the system bandwidth, and M is the modulation order. When the system transmit power is normalized to one, the noise power given by σ^2 corresponding to a specific E_b/N_0 can be generated by

$$\sigma^2 = \frac{N_0}{E_b}$$

In the first simulation, the performance of synchronization and channel estimation are investigated in the MB OFDM system. As shown in Figures 3.15-3.18, the bit error rate (BER) of different modes in the CM4 channel decreases with increase in E_b/N_0 except for the 480 Mbps data rate mode. Figure 3.18 depicts that BER of the 480 Mbps data rate mode has an error floor resulting from the influence of ICI, because the mode has no strategy for combating the ICI such as spreading or low coding rate. In the next simulation we will investigate the ICI compensation methods.

In the second simulation, the performances of ICI compensation methods are investigated in the MB OFDM system. The ICI induced by the multipath energy outside the FFT window is depicted and the ICI-to-signal ratio is shown in Figure 3.19. To capture sufficient multipath energy and minimize the impact of ICI, the ZPP duration was chosen to be 60.6 ns by the MB OFDM system according to the CM3 channel. As shown in Figure 3.19, the ZPP duration is sufficient to minimize the impact of ICI for CM1-CM3 channels, but not for the CM4 channel. Figure 3.20 shows the uncoded BER versus number of iterations with DAIC for the CM4 channel; it depicts that performance of the uncoded BER is clearly improved after a single iteration is done. (Synchronization and channel estimation at the receiver are assumed to be perfect.) However, the performance of the uncoded BER will be improved less and less as the number of iterations increases. According to Figure 3.20, we consider that three iterations are enough for the MB OFDM system in the CM4 channel. Figure 3.21 depicts the BER of the 480 Mbps data rate mode in the CM4 channel as a function of E_b/N_0. The BER of the conventional method has an error floor due to the impact of ICI. However, the MMSE equalizer and the DAIC

method can improve the performance of the BER significantly. The curve illustrates that the MMSE equalizer in the CM 4 channel gains 1 dB for a BER of 10^{-3} compared with the DAIC method.

Now, we compare the LS channel estimation with the DAIC channel estimation. The MSE of two channel estimation techniques in the CM4 channel are shown in Figure 3.22. It shows that the DAIC channel estimation is more accurate than the LS channel estimation at high E_b/N_0. However, the MSE of the DAIC channel estimation is higher than the LS channel estimation at low E_b/N_0. This is because that errors are dominated by the noise at low E_b/N_0, such that the DAIC channel estimation cannot correctly reconstruct the influence of ICI and thus results in the error propagation. As shown in Figure 3.23, the BER performances of the MMSE equalizer and the DAIC method with the LS channel estimation have an error floor. This is because that the LS channel estimation cannot eliminate the ICI, such that the two methods cannot work correctly without the accurate estimated channel. On the other hand, the BER performances of the MMSE equalizer and the DAIC method with the DAIC channel estimation show significant improvement compared with that obtained by the LS channel estimation.

3.7 Summary

In this chapter, we first introduced the indoor UWB channel model and the receiver architecture of the MB OFDM system. The main difference between UWB channel and general narrow-band channel is the “cluster” phenomenon due to the high resolution resulting from large bandwidth of UWB waveforms. There are four channel models defined for various LOS and NLOS environments. In addition, the conventional OFDM receiver techniques like synchronization and channel estimation are then introduced. It is found that the long delay spread in the CM4 channel will

induce the ICI effect and degrade the system performance.

In MB OFDM systems, the ZPP duration chosen to be 60.6ns is enough to capture sufficient multipath energy and minimize the impact of ICI for the CM1-CM3 channels, but not the CM4 channel. For those modes with time-domain spreading, like 106.7 Mbps and 200 Mbps, the MRC is effective to suppress the effect of ICI. In addition, the MMSE equalizer can deal with the influence of ICI for the modes without any spreading, like the 320 Mbps and 480 Mbps modes. However, the high complexity of the channel matrix inversion computation is not suitable for the MB OFDM system. We thus propose the simplified DAIC method to eliminate ICI. The simulation results show that the proposed method can alleviate the influence of the ICI and improve the BER performance in the CM4 channel. More importantly, the proposed method has lower complexity than the MMSE equalizer. It is found that the LS channel estimation is not suitable for the CM4 channel. Due to that the two OFDM training symbols suffer the same influence by ICI, the LS channel estimation cannot perform reliably under the CM4 channel. This prompts us to develop the DAIC method to estimate the channel impulse response. The simulation results indicate that the DAIC channel estimation effectively eliminates the effect of ICI and is more accurate than the LS channel estimation.

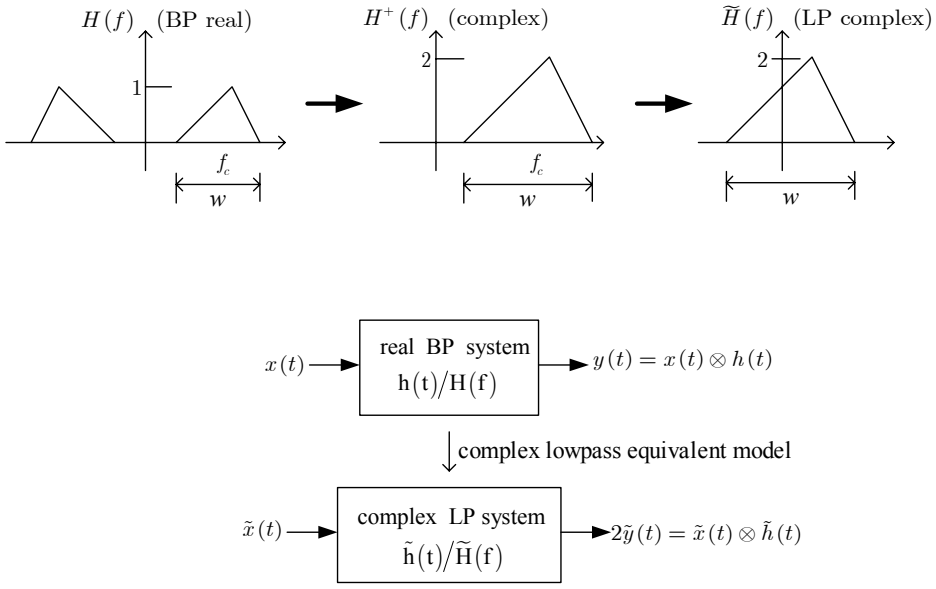

Figure 3.1: Simulation of passband system in terms of equivalent complex baseband system

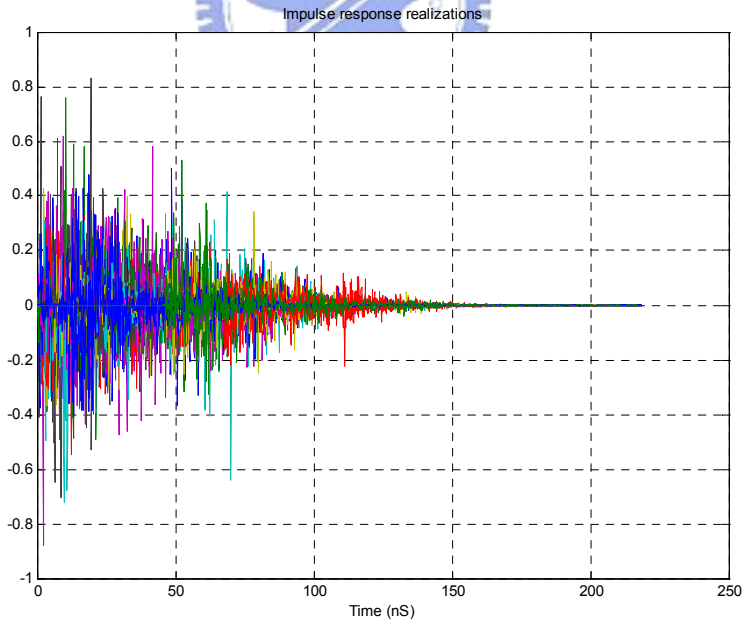

Figure 3.2: 100 impulse responses based on the CM3 channel model (NLOS up to 10 m with average RMS delay spread of 15 ns)

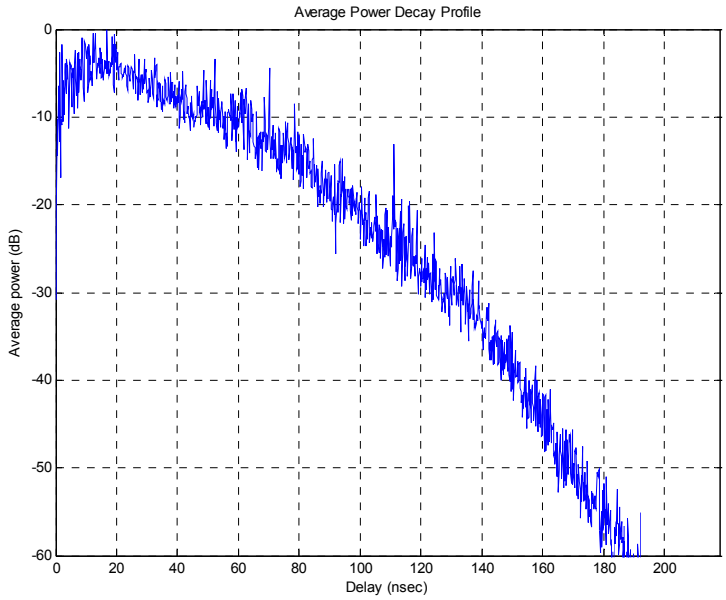

Figure 3.3: Average power decay profile for the channel model CM3 (NLOS up to 10 m with average RMS delay spread of 15 ns)

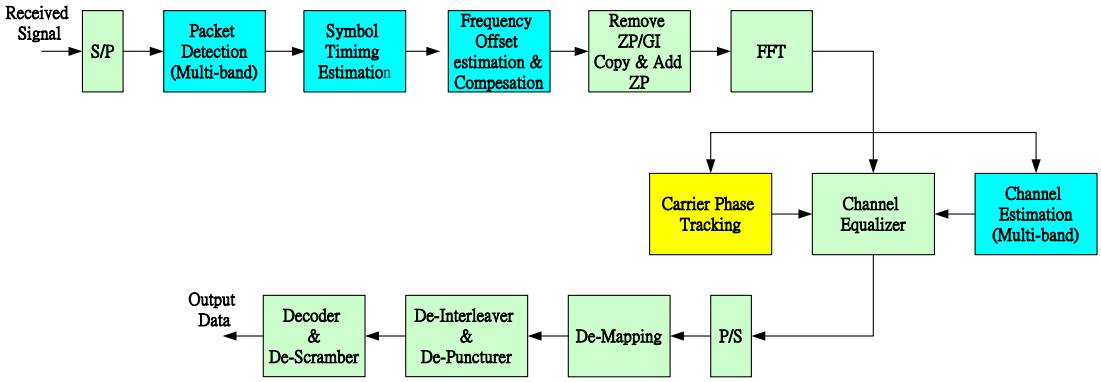

Figure 3.4: Block diagram of the MB OFDM receiver

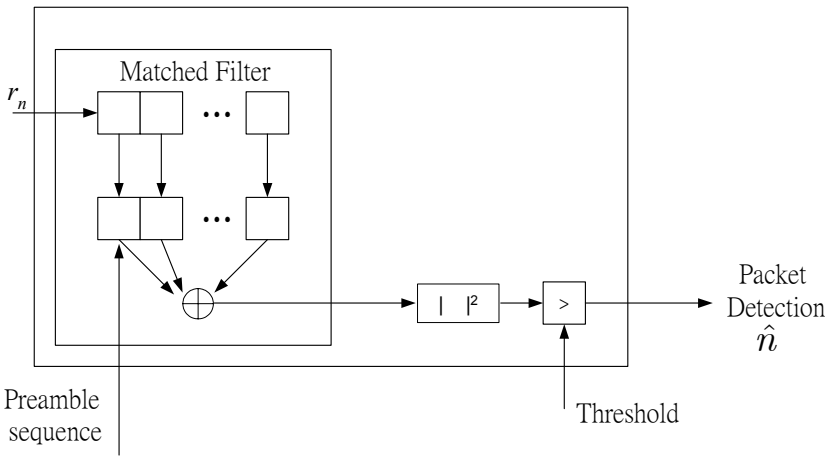

Figure 3.5: Block diagram of the cross-correlation packet detection

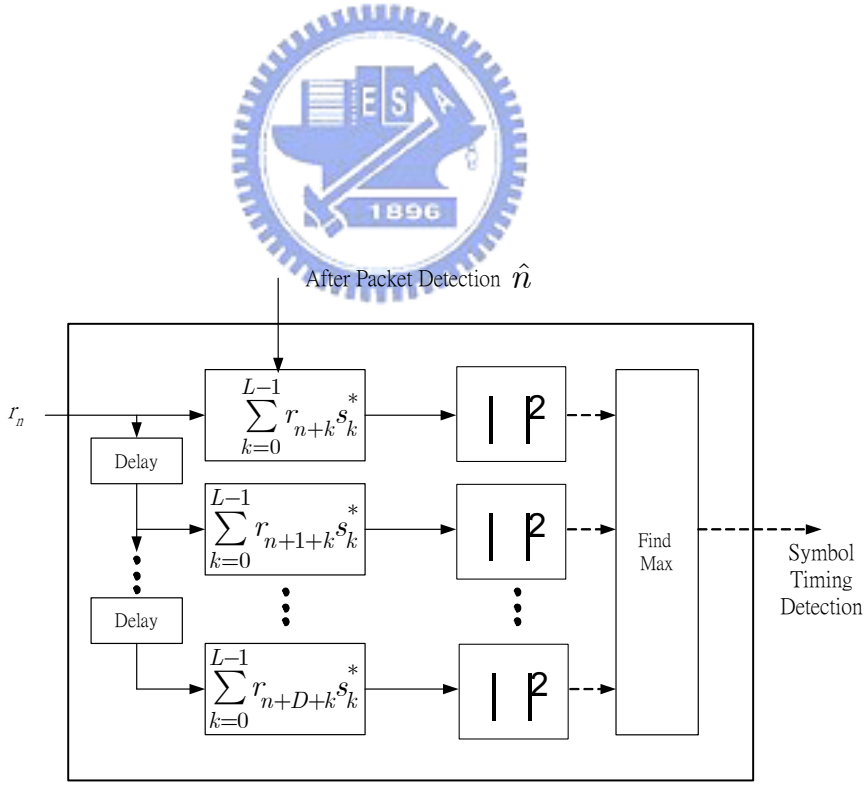

Figure 3.6: Block diagram of the symbol timing estimation

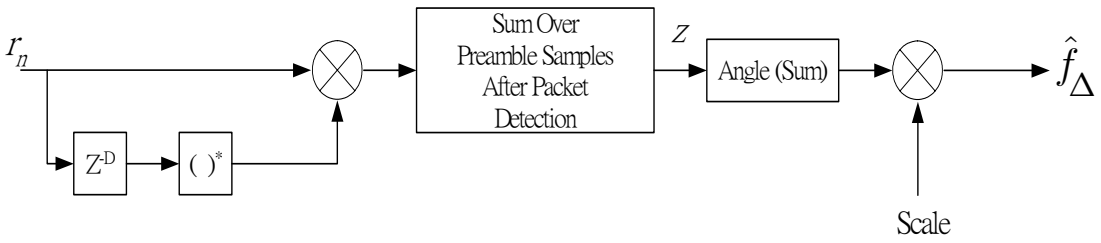

Figure 3.7: Block diagram of the frequency synchronization estimation

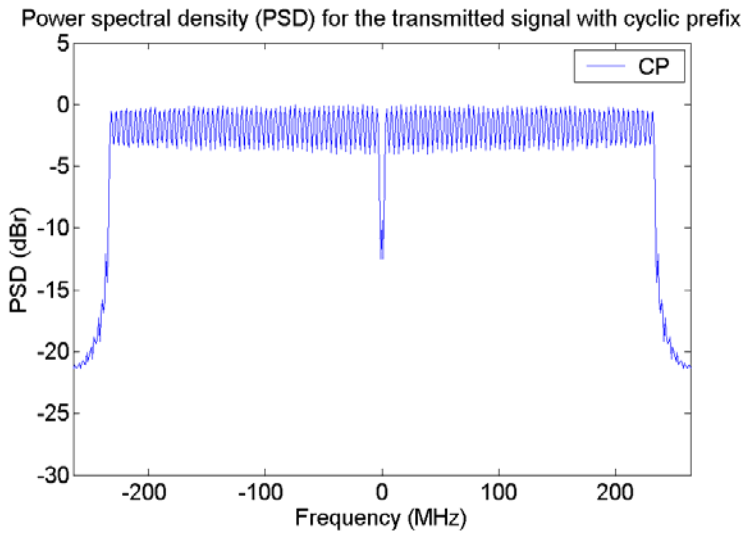

Figure 3.8: PSD plots for the OFDM system using CP prefix

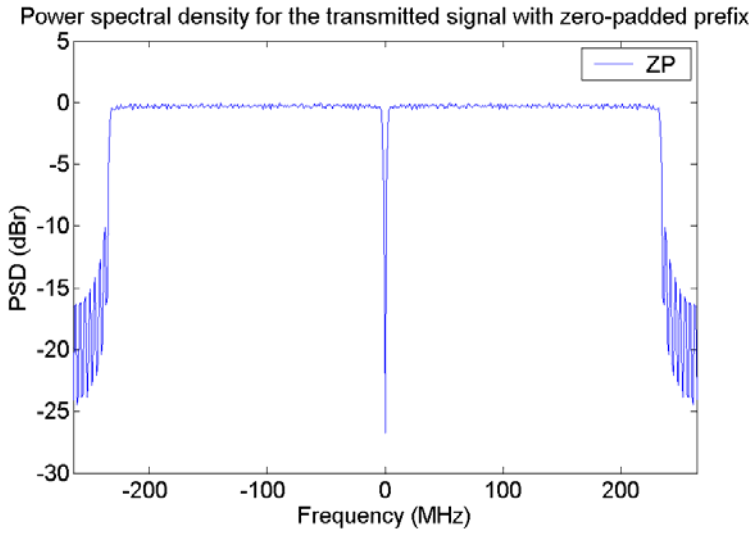

Figure 3.9: PSD plots for the OFDM system using ZPP

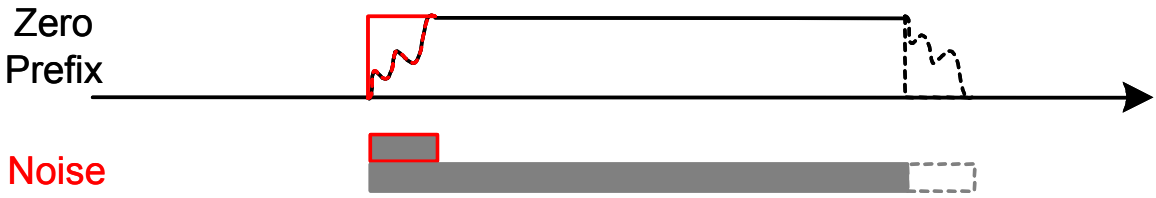

Figure 3.10: The ZPP OFDM system pick up larger noise at receiver

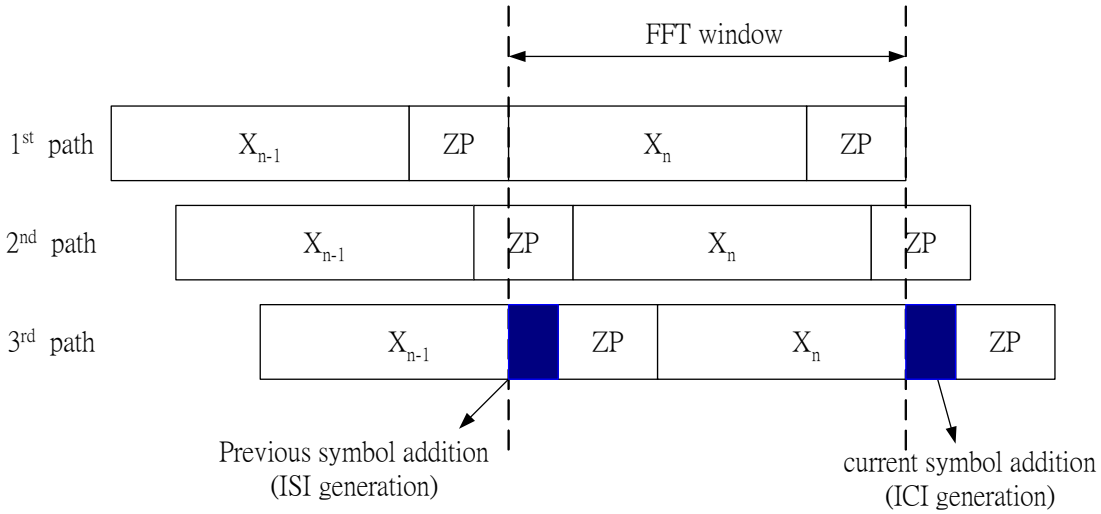

Figure 3.11: Illustration of ISI and ICI due to long delay path

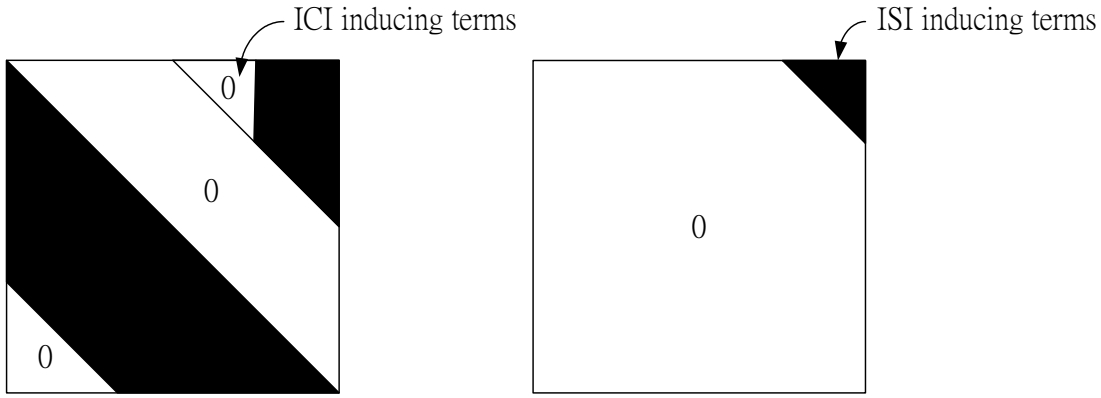

Figure 3.12: Illustration of ISI (right) and ICI (left) channel matrix shapes

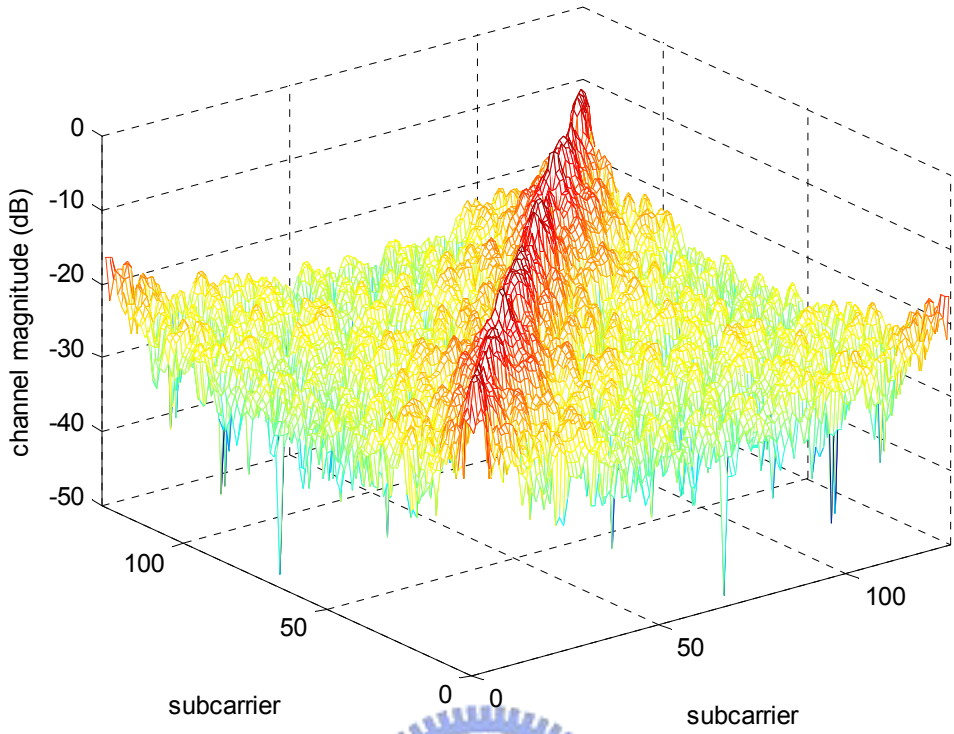

Figure 3.13: Magnitude of ICI matrix in frequency domain

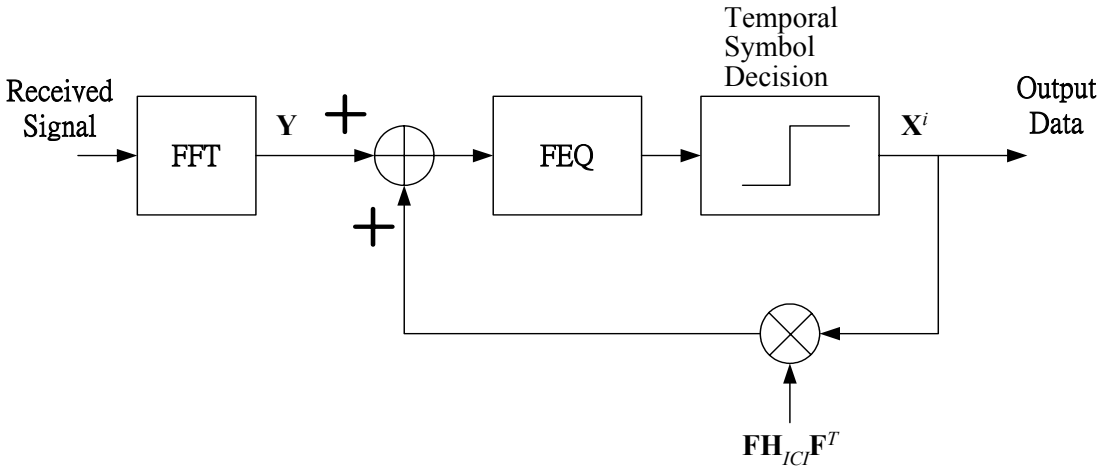

Figure 3.14: Block diagram of the decision-aided ICI canceller

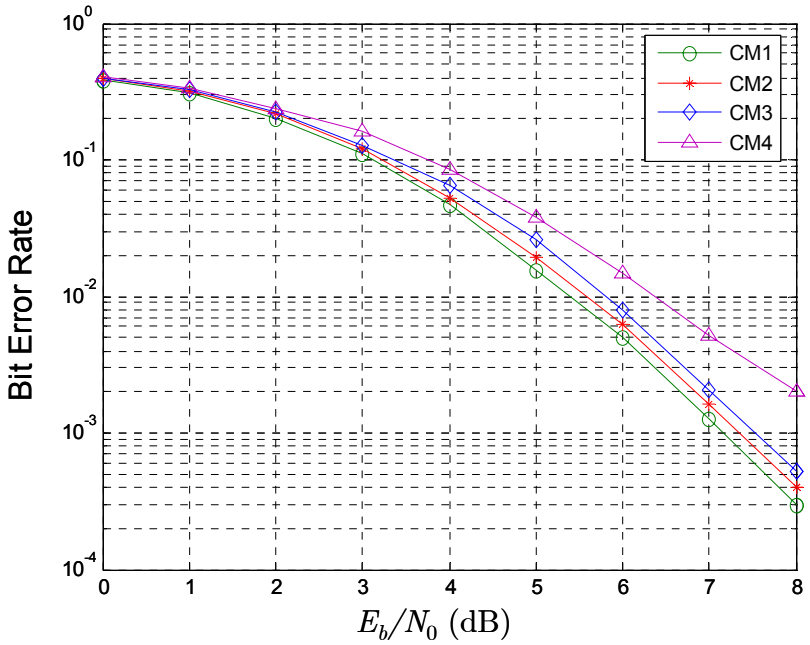

Figure 3.15: Coded BER as a function of E_b/N_0 for 53.3 Mbps data rate of the MB OFDM system in CM1-4 channels with parameters estimation

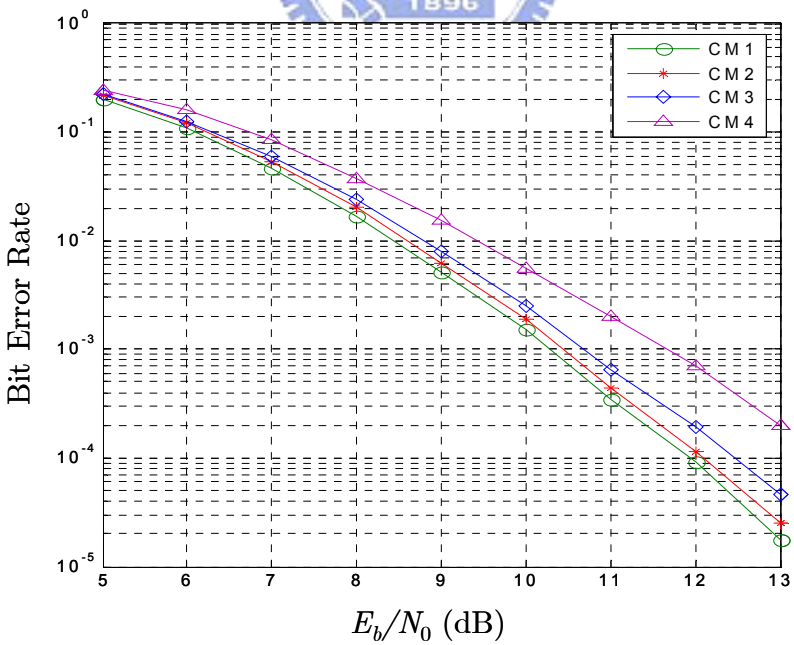

Figure 3.16: Coded BER as a function of E_b/N_0 for 106.7 Mbps data rate of the MB OFDM system in CM1-4 channels with parameters estimation

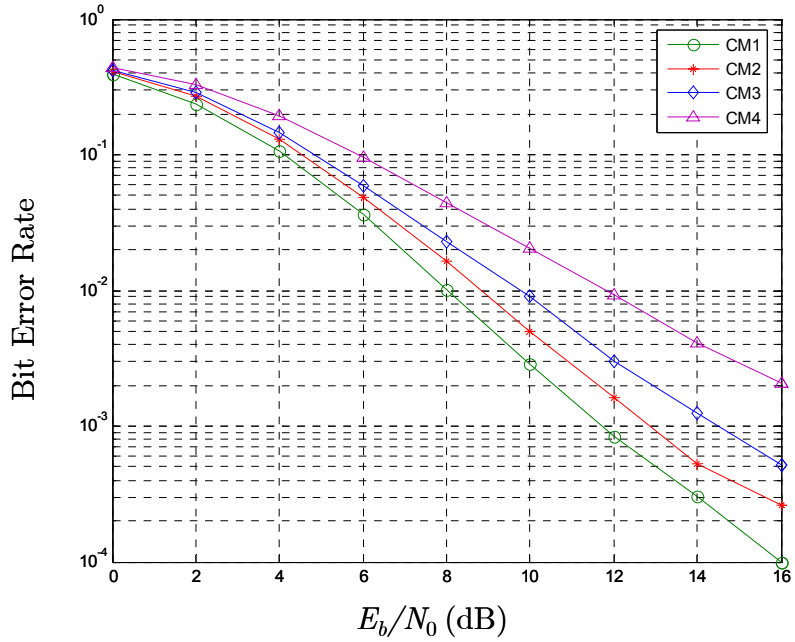

Figure 3.17: Coded BER as a function of E_b/N_0 for 200 Mbps data rate of the MB OFDM system in CM1-4 channels with parameters estimation

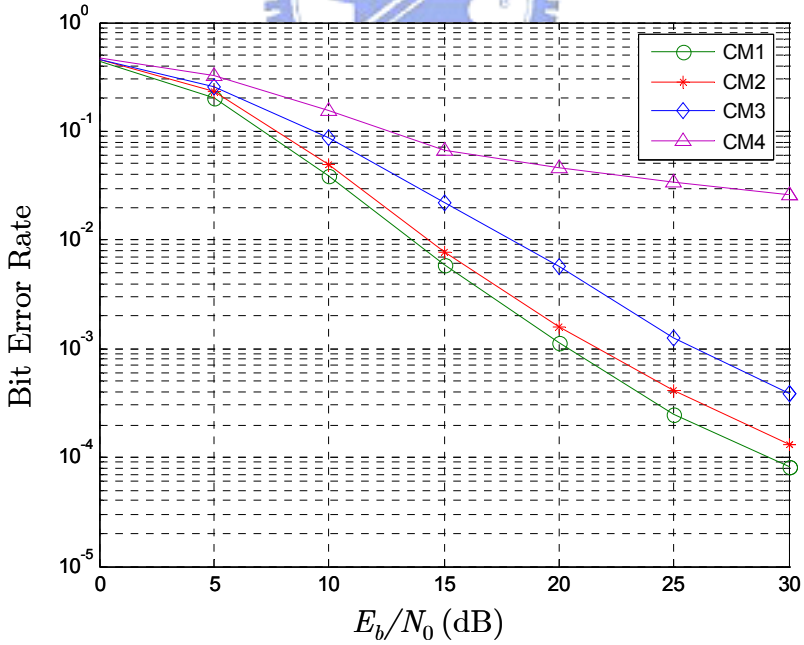

Figure 3.18: Coded BER as a function of E_b/N_0 for 480 Mbps data rate of the MB OFDM system in CM1-4 channels with parameters estimation

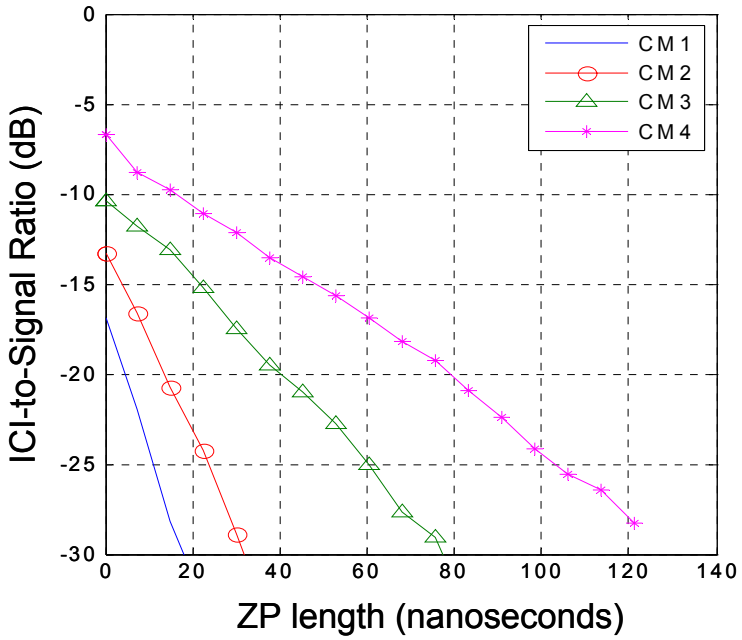

Figure 3.19: Captured multipath energy as a function of ZPP length for CM1-4 channels

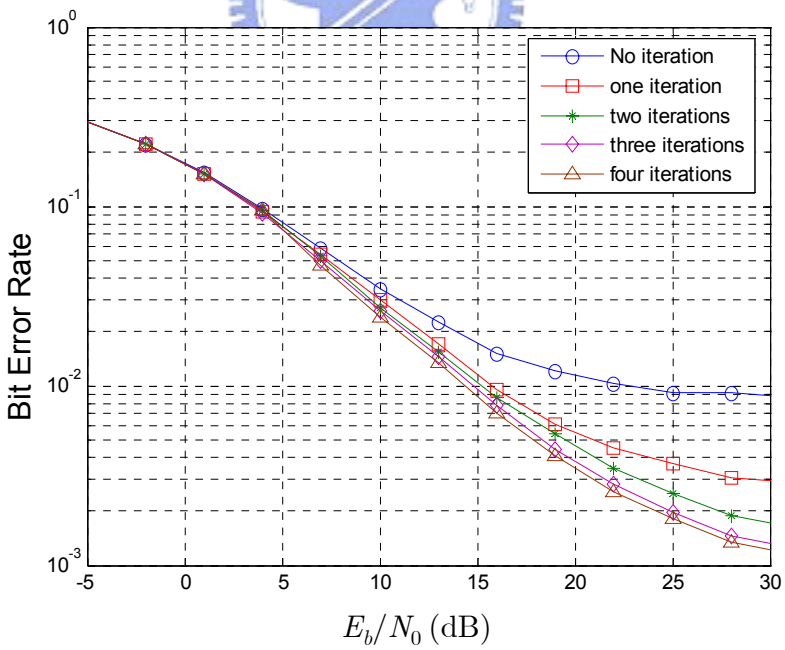

Figure 3.20: Uncoded BER versus E_b/N_0 with different iteration number in the CM4 channel

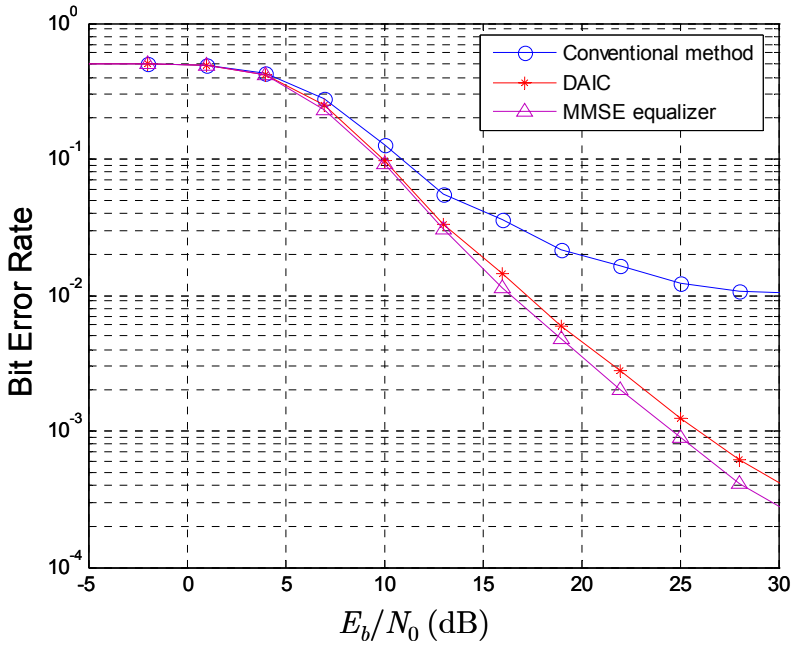

Figure 3.21: Coded BER as a function of E_b/N_0 for 480 Mbps data rate of the MB OFDM system in the CM4 channel

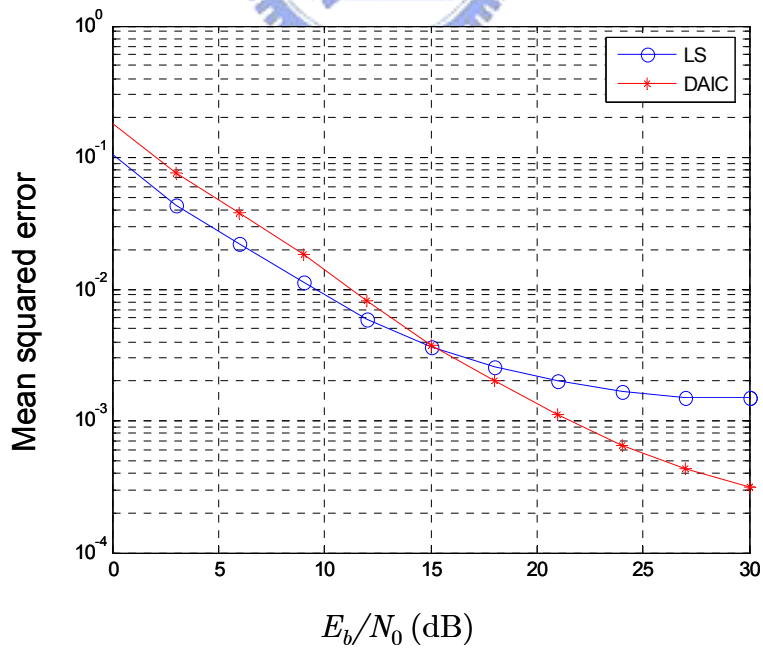

Figure 3.22: Mean square estimation error of the CM4 channel frequency response

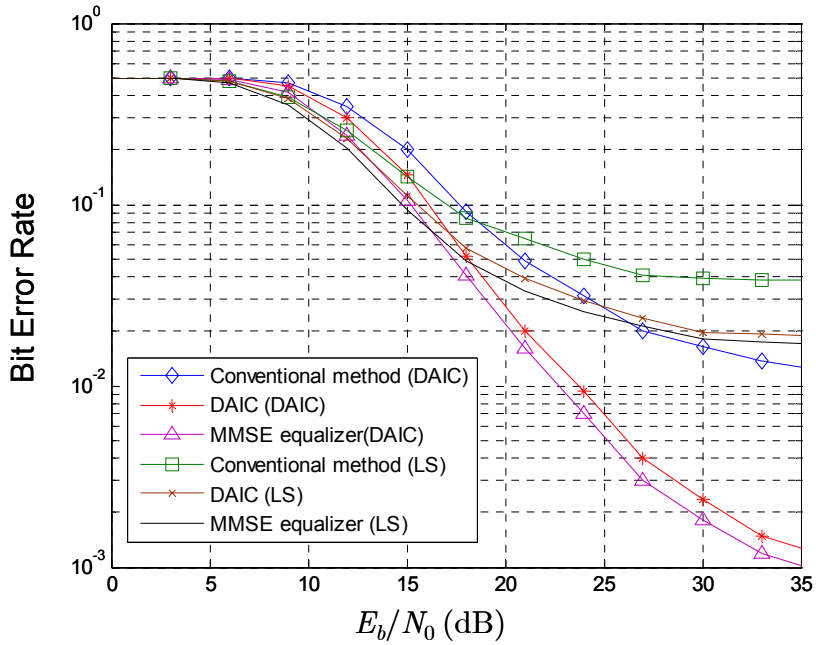

Figure 3.23: Coded BER versus E_b/N_0 for 480 Mbps data rate of the MB OFDM system in the CM4 scenario with estimated channel impulse response

Table 3.1: Multipath channel target characteristics and model parameters.

Target Channel Characteristics	**CM 1**	**CM 2**	**CM 3**	**CM 4**
Mean excess delay (nsec) (τ_m)	5.05	10.38	14.18	
RMS delay (nsec) (τ_{rms})	5.28	8.03	14.28	25
NP_{10dB}			35	
NP (85%)	24	36.1	61.54	
Model Parameters				
Λ (1/nsec)	0.0233	0.4	0.0667	0.0667
λ (1/nsec)	2.5	0.5	2.1	2.1
Γ	7.1	5.5	14.00	24.00
γ	4.3	6.7	7.9	12
σ_1 (dB)	3.3941	3.3941	3.3941	3.3941
σ_2 (dB)	3.3941	3.3941	3.3941	3.3941
σ_x (dB)	3	3	3	3
Model Characteristics				
Mean excess delay (nsec) (τ_m)	5.0	9.9	15.9	30.1
RMS delay (nsec) (τ_{rms})	5	8	15	25
NP_{10dB}	12.5	15.3	24.9	41.2
NP (85%)	20.8	33.9	64.7	123.3
Channel energy mean (dB)	-0.4	-0.5	0.0	0.3
Channel energy std (dB)	2.9	3.1	3.1	2.7

Chapter 4

Interference Avoidance Transmission Scheme for IEEE 802.15.3a Multi-band OFDM

Due to the lack of coordination of transmissions among different piconets, the conventional multiple accesses are not suitable for multi-piconet environments. In this chapter, the multiple access techniques for intra- and inter-piconet of the IEEE 802.15.3a MB OFDM system will be introduced first. Then, the collision characteristics of SOP will be introduced in the following section. In addition, the interference avoidance transmission scheme will be described. Finally, the performance simulations are shown in Section 4.5.

4.1 Review of Multiple Access Techniques

Three of the major basic multiple access techniques for wireless communications will be reviewed: first is frequency division multiple access (FDMA), second is time division multiple access (TDMA), third is code division multiple access (CDMA) [31].

In FDMA systems, the frequency-time plane is partitioned into non-overlapping frequency bands. Each of them serves a single user. Every user is therefore equipped

with a transmitter for a given, predetermined, frequency band, and a receiver for each band which can be implemented as a single receiver for the entire range with a bank of bandpass filters for the individual bands. The spectral regions between adjacent channels are called guard bands, which help reduce the interference between channels. FDMA is used exclusively for analog cellular systems, even though FDMA can be used for digital systems in theory. Essentially, FDMA splits the allocated spectrum into many subchannels. The main advantage of FDMA is its simplicity. It doesn't require any coordination or synchronization among users since each user can use its own frequency band without interference. However, this is also the cause of waste especially when the load is momentarily uneven since when one user is idle his share of bandwidth can't be used by other users. It should be noted that if the users have uneven long term demands, it is possible to divide the frequency range unevenly, i.e., proportional to the demands. However, FDMA is not flexible when adds a new user to the network requiring equipment modification, such as additional filters, in every other user. The key advantages of FDMA can be summarized as follows:

1. Easy implementation
2. Small intersymbol interference

The disadvantages of FDMA can also be summarized as follows:

1. Low flexibility in channel allocation
2. Small channel capacity in cellular system

In TDMA systems, sharing of the communication resource is accomplished by dividing the frequency-time plane into non-overlapping time slots which are transmitted in periodic bursts. Every user is allowed to transmit freely during the time slot assigned to him, that is, the entire system resources are devoted to that user during the assigned time slot. Time is segmented into intervals called frames. Each frame is further partitioned into user assignable time slots. An integer number of time

slots constitutes a burst time or burst. Guard times are allocated between bursts to prevent overlapping of bursts. Each burst is comprised of a preamble and the message portion. The preamble is the initial portion of a burst used for carrier and clock recovery, station identification, and other housekeeping tasks. The message portion of a burst contains the coded information sequence. In some systems, a training sequence is inserted in the middle of the coded information sequence. The advantage of this scheme is that it can aid the receiver in mitigating the effects of the channel and interference. The disadvantage is that it lowers the frame efficiency; that is, the ratio of the bit available for messages to the total frames length.

The TDMA systems are designed for use in a range of environments and situations, form hand portable using in a downtown office to a mobile user traveling at high speed on the freeway. It also supports a variety of services for the end user, such as voice, data, fax, short message services, and broadcast messages. TDMA offers a flexible air interface, providing high performances in capacity, coverage, mobility, and capability to handle different types of user needs. While TDMA is a good digital system, it is still somewhat inefficient since it has no flexibility for varying data rates and has no accommodations for silence in telephone conservation. TDMA also requires strict signaling and timeslot synchronization. A point worth noting is that both FDMA and TDMA system performances degrade in the presence of the multipath fading. More specifically, due to the high data rates of TDMA systems, the time dispersive channel (a consequence of delay spread phenomenon) causes intersymbol interference (ISI). This is a serious problem in TDMA systems thus requiring adaptive techniques to maintain system performance. The key advantages of TDMA can be summarized as follows:

1. Sharing single carrier frequency with multiple users.
2. Non-continuous transmission makes handoff simpler. It means that mobile assisted handoff is possible.

3. Less stringent power control due to the reduced interuser interference.
4. Slots can be assigned on demand (concatenation and reassignment). It means that bandwidth can be supplied on demand.

The disadvantages of TDMA can also be summarized as follows:

1. High synchronization overhead is needed.
2. Equalization is necessary for high data rates.
3. Power envelop will pulsate. It is caused by interfering with other devices.
4. High frequency/slot allocation complexity is needed.

As is clear from the above simple review, in both FDMA and TDMA techniques the number of channels or time slots is fixed for a given system, and a signal channel is allocated to a single user for the whole period of communications. Having a fixed channel or time slot assignment could guarantee the service quality for real-time and constant-bit-rate voice telephony, the main service at that time. However, fixed channel assignment has displayed its lack of efficiency in utilizing the scarce spectrum, particularly with the number of users increasing. CDMA gives a good solution for the problem of efficiency. In a CDMA system the original narrowband user's information is spread into a much wider spectrum with a high chip rate. Because each user uses a different uncorrelated code, it is possible to send multiple user's information on the same frequency spectrum without serious interference in detecting the desired signal at the receiver as long as the correct spreading code is known to the receiver. The signal from each user will have very low power and be seen by other as background noise. Consequently, as long as the total power of noise and multi-user interference is less than a threshold, the information signal can be recovered by correlating the received spread signal with a synchronized replica of the spreading signal. The key advantages of CDMA can be summarized as follows:

1. The system capacity improvement is mainly contributed by improved coding gain.
2. The average transmitted power is less than the average power typically required

by TDMA.

3. CDMA provides robust operation in fading environments by using a Rake receiver.

The disadvantages of CDMA can also be summarized as follows:

1. Requirement for power control.
2. Requirement for long overhead for synchronization.

4.2 Multiple Access in Multi-band OFDM System

IEEE 802.15.3a defines the piconet as the wireless ad hoc data communications system and it allows a number of independent data devices to communicate with each other [32][33]. The communication range of a piconet is usually confined to the area around person or object which covers about 10 m in all directions and surrounds the person or a device. The piconet consists of several components, as shown in Figure 4.1 [32]. The basic component is the devices. Some device is required to occupy the role of the piconet coordinator (PNC) of the piconet. The PNC provides the timing of the piconet with the beacon. In addition, the PNC controls the QoS requirements, power save modes and access control to the piconet.

The IEEE 802.15.3a MB OFDM system has two type of multiple access. TDMA is used for devices within one piconet. In addition, different piconets which can operate in the same area are distinguished by the use of different TFICs. In the following, the multiple access of intra- and inter-piconet will be introduced.

4.2.1 Time Division Multiple Access (TDMA) for Intra-Piconet Interference Reduction

According to the Specification of the IEEE 802.15.3, timing in the 802.15.3 piconet is based on the superframe. As shown in Figure 4.2 [32], the superframe is composed of three parts:

1. The beacon: it set the timing allocations and communicates management information for the piconet. The beacon consists of the beacon frame and any announce commands sent by the PNC as a beacon extension.
2. The contention access period (CAP): it communicates commands and/or asynchronous data if it is present in the superframe.
3. The channel time allocation period (CTAP): it is composed of channel time allocations (CTAs), which also include management CTAs (MCTAs). Commands, isochronous streams and asynchronous data connections are transmitted in the CTAP.

The PNC will determine the length of the CAP and communicate to the devices in the piconet via the beacon. However, the PNC is capable of replace the functionality provided in the CAP with MCTAs. MCTAs are also one type of CTA for communications between the devices and the PNC. The CAP uses carrier sense multiple access with collision avoidance (CSMA/CA) for the medium access. In addition, the CTAP uses a standard TDMA protocol and all devices have specified time windows.

4.2.2 Time-Frequency Interleaving Codes for Inter-Piconet Interference Reduction

For the MB OFDM system, the performance of a piconet in the presence of other piconet is an important design consideration. The SIR will determine the performance and it is given as

$$\mathrm{SIR} = \left(\frac{P_{\mathrm{sig}}}{P_{\mathrm{int}}}\right)\left(\frac{W}{R}\right) \tag{4.1}$$

where P_{sig} is the power of the desired signal, P_{int} is the power of the interference, R is the information data rate, and W is the effective bandwidth of the transmitted signal. The first term in Equation 4.1 is the distance separation between the two piconets, while the second term in the Equation 4.1 is indicated as bandwidth expansion factor and is the processing gain available to suppress the interference. In the MB OFDM system, the effective bandwidth is defined as follows:

$$W = \frac{N_B \times N_{DT}}{T_s} \tag{4.2}$$

where N_B is the number of bands, N_{DT} is the number of data tones, and T_s is the symbol duration. From the above discuss, there are two methods to improve performance in the presence of other piconet interference. The first method is to guarantee that there is a sufficient separation between the reference devices and the interfering devices. However, it is impossible to maintain the distance between devices of two piconets in practical applications. The second method is to make the bandwidth expansion factor as large as possible.

There are some ways to achieve bandwidth expansion. The two most well-known techniques are time- and frequency-domain spreading and coding. In addition to the previous two approaches, the MB OFDM system uses the time–frequency interleaving approach to obtain bandwidth expansion: As shown in Figure 4.3, the information data is expanded in bandwidth by the three methods.

According to the requirement for a UWB system, the MB OFDM system has to support up to four piconets, which will overlap between each other. Due to the spreading and coding techniques are the same for four piconets. Consequently, the only way to distinguish one piconet from the other is to specify four unique

time–frequency interleaving codes

4.3 Simultaneously Operating Piconets (SOP)

However, when overlapped multiple piconets occur, there is no coordination of transmissions among different piconets. Thus, the MB OFDM system must possess robustness to mitigate the interference from other piconets. In the following section, we will introduce the goals in the design of the TFICs [34]-[36].

4.3.1 Collision Characteristics

There are two destinations for the design of the time–frequency interleaving codes. First, the average number of collisions between any two time–frequency interleaving codes must be 1/3 as shown in Figure 4.4. The other is that the collisions should be uniform distribution for all shifts of the codes. According to two goals, four time–frequency codes, which are listed in Table 2.6, have been designed.

4.3.2 Interference Avoidance Transmission Scheme for SOP

According to Specification of IEEE 802.15.3, the PNC should periodically listen in the current channel to detect interference resulting from the presence of other 802.15.3a piconets or the presence of other wireless networks. When there are other piconets detected by the PNC, four methods that are available to mitigate the interference between the two piconets are listed as follow

1. The PNC may join the other piconet to form a child piconet.
2. The PNC may join the other piconet to form a neighbor network.
3. The PNC may change channels to one that is unoccupied.

4. The PNC may reduce the maximum transmit power in the piconet.

The first two methods can complete avoid the interference due to two piconets become one piconet. However, the last two methods are not suitable for the MB OFDM system. Because signals of interference piconet exist in all channels and they still influence the desired piconet even though the desired piconet reduces the transmit power. To further improve performance in presence of other piconet, we propose an interference avoidance transmission scheme. The MB OFDM system employs the preamble to aid receiver algorithms related to synchronization, carrier-offset recovery, and channel estimation. We can exploit the property to find other piconet, when other piconet has existed in the frequency slots of the desired piconet based on the specific time-frequency interleaving pattern.

First, the desired PNC will listen to channels according to the specific time-frequency interleaving pattern. The desired PNC will calculate the cross-correlation of two successive signals in the same frequency slot. The *l*th received signal of an *L*-length window integrate-and-dump cross-correlator is

$$P_l = \mathbf{r}_l^H \mathbf{r}_{l+1} \tag{4.3}$$

where $\mathbf{r}_l = [r_0, r_1, ..., r_{L-1}]^T$ and $[\cdot]^H$ denotes Hermitian transpose. Further, normalizing $|P_l|$ produces the correlation coefficient

$$|\rho_l| = \frac{|P_l|}{\sqrt{R_l R_{l+1}}} \tag{4.4}$$

where $R_l = \mathbf{r}_l^H \mathbf{r}_l$ and the range of $|\rho_l|$ is constrained to [0 1]. The receiver will declare the interference detection at the frequency slot when some threshold of correlation T_c is exceeded, that is, when $|\rho_l| > T_c$. The commonly used value of T_c = 0.8 [37].

When other piconet has existed in the frequency slots of the desired piconet, the

desired PNC has to know how many portions of each frequency slot are overlapped with the frequency slot of the interference piconet. Consequently, we divide the each desired frequency slot into several smaller time-frequency slots, as shown in Figure 4.5. Then, we also calculate the correlation coefficient of each time-frequency slot in the desired frequency slots which have been detected the presence of interference piconet. Similarly, if the time-frequency slot in the desired frequency slots is overlapped with the frequency slost of the interference piconet, the threshold of correlation T_c is exceeded. By counting the number of time-frequency slots covered with frequency slots of the interference piconet, the PNC can find out the portions of each frequency slot overlapped with the frequency slots of the interference piconet. According to the above result, the PNC can decide the shift time which makes the each frequency slot of two piconets totally separate or cover with each other. After adjusting the time of the desired frequency slot in the time axis, there are only two desired frequency slots with other piconet interference. The other frequency slots are interference-free for the desired piconet. Additionally, if the interference piconet has existed in this area, the desired piconet cannot occupy the frequency slots of the interference piconet. For this reason, the desired piconet will close down the two frequency slots jammed by other piconet. The devices in the desired piconet will transmit signals with the remainder of the frequency slots. Figure 4.6 presents the flow chart of the interference avoidance for desired piconet

For example, the desired piconet uses the time-frequency interleaving pattern {f1, f3, f2, f1, f3, f2, repeats}, whereas the interference piconet uses the time-frequency interleaving pattern {f1, f2, f3, f1, f2, f3, repeats}. As shown in Figure 4.4, the signal of the interference piconet and the desired piconet are not time-aligned due to the lack of coordination of transmissions among two piconets. Collisions will occur between two piconets. At worst case, there are four frequency

slots occurred collisions between two piconets, so that the desired piconet may not decode the signal correctly. By means of the correlation coefficient of each time-frequency slot, the desired piconet shifts its own specific time-frequency interleaving pattern in the time axis. Therefore, there are only two frequency slots overlapped with the interference piconet, as shown in Figure 4.7. And the desired piconet turns off the two frequency slots. Because the MB OFDM system improves the performance of SOP by all three techniques: spreading, convolutional code and TFIC. We consider the binary information bits of desired piconet are encoded with a coding rate of 1/3 in 106.7 Mbps mode as shown in Figure 4.8. Each 200 coded-bit output of each generator polynomial of the encoder is interleaved, mapped into one of QPSK constellation points and OFDM-modulated by 128-points IFFT. Each OFDM symbol is transmitted twice at different frequency slots based in the specific time-frequency interleaving pattern. When 1st and 4th frequency slots have been turned off, the transmission method which keeps the coding rate (1/3) and loses partial frequency diversity is shown in Figure 4.9. The first 200 coded-bit can be received from 2nd OFDM symbol and the second 200 coded-bit can be received from 3rd OFDM symbol. In addition, the third 200 coded-bit can be received from coherently combining 5th and 6th OFDM symbols. Consequently, the third 200 coded-bit can maintain the frequency diversity. Then, the receiver can decode the desired signal correctly.

4.4 Computer Simulations

Computer simulations are conducted to evaluate the performance of the interference avoidance transmission scheme in the MB OFDM system. Because the MB OFDM system uses spreading, coding and TFICs to improve the performance of SOP, we consider the 106.7 Mbps data rate mode which has enough redundancy to allow the receiver to decode the desired signals correctly in the presence of other piconets.

In the first simulation, the performance of the interference avoidance transmission scheme is investigated with different numbers of time-frequency slots in each frequency slot. The ideal case means that the transmitter conveys signals with four interference-free frequency slots and the signals are not jammed by other piconets In addition, the MRC case means that the transmitter conveys signals with six frequency slots and the receiver decodes the signals by MRC. The BER performances of the proposed method with different number of time-frequency slots in each frequency slot in the CM1-2 channels are shown in Figures 4.10-4.11. They show that the BER associated with eight time-frequency slots in each frequency slot is close to the ideal case. This means that the proposed method with eight time-frequency slots in each frequency slot can avoid most of the interference from other piconets. In addition, the BER associated with two or four time-frequency slots in each frequency slot have an error floor, implying the two and four divisions are not enough. This is because the more time-frequency slots are divided in a frequency slot, the more accurately we can shift to the desired position, and the less severely the collision due to the inaccurate shift will occur.

In the second simulation, the performance of the interference avoidance transmission scheme is investigated with different SIR. Each frequency slot is

divided into eight time-frequency slots. The BER performances of the proposed method with different SIR in the CM1 channel are shown in Figure 4.12. The curve illustrates that the proposed method with SIR = −10 dB only loses 2.5 dB for a BER of 10^{-4} compared with the ideal case. This means that the proposed method can effectively mitigate the interference even if the interference is larger than the desired signal.

4.5 Summary

In the MB OFDM system, TDMA is used for devices within the same piconet. However, the conventional multiple accesses are not suitable for multi-piconet environments due to the lack of coordination of transmissions among different piconets. In order to improve the performance under SOP, the MB OFDM system uses three methods, spreading, convolutional code, and TFICs, to achieve bandwidth expansion to alleviate the interference. In practice, the performance of SOP will be seriously degraded when the power of other piconets is high. To further improve the performance of SOP, we proposed the interference avoidance transmission scheme. When other piconets are present in the same area, the desired piconet will convey the signals in the interference-free frequency slots. By partially abandoning frequency diversity, the transmitter can keep the original coding rate which is shown to be able to significantly improve the performance of SOP. The simulation results indicate that the proposed scheme effectively alleviates the interference from other piconets and the resulting BER performance is close to the ideal case.

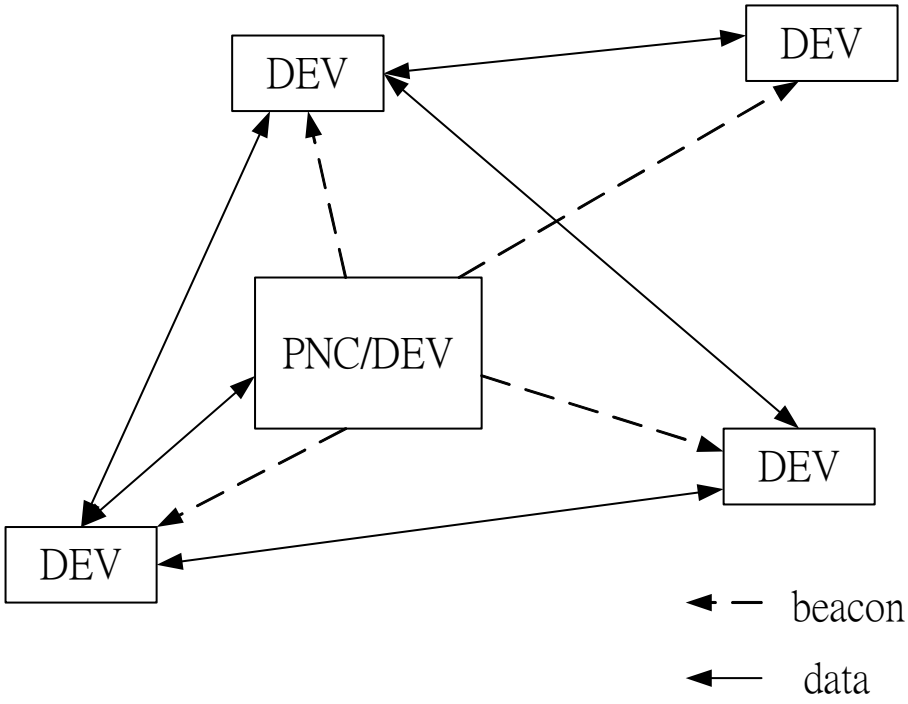

Figure 4.1: The 802.15.3 piconet elements

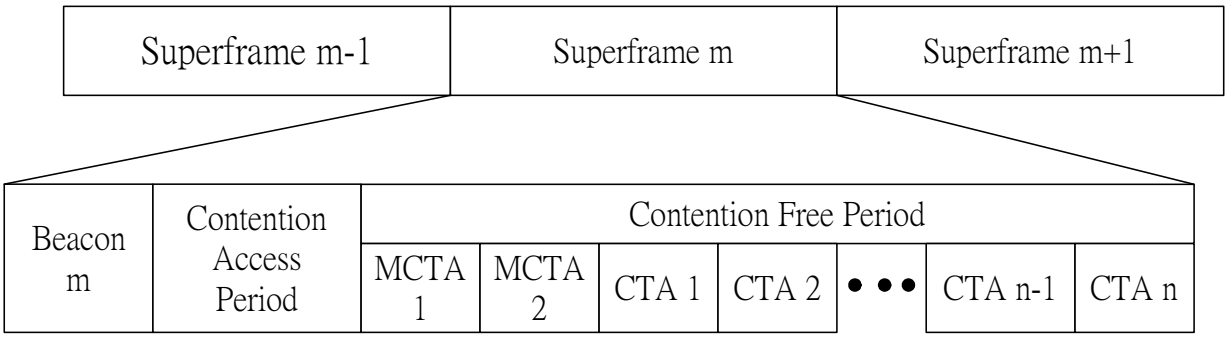

Figure 4.2: The 802.15.3 piconet superframe

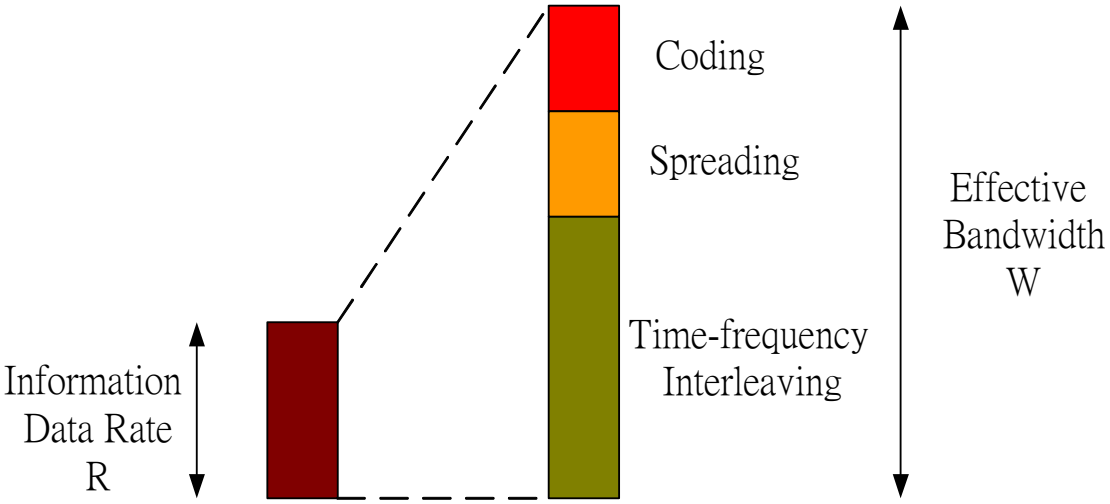

Figure 4.3: Pictorial representation of bandwidth expansion for the MB OFDM system

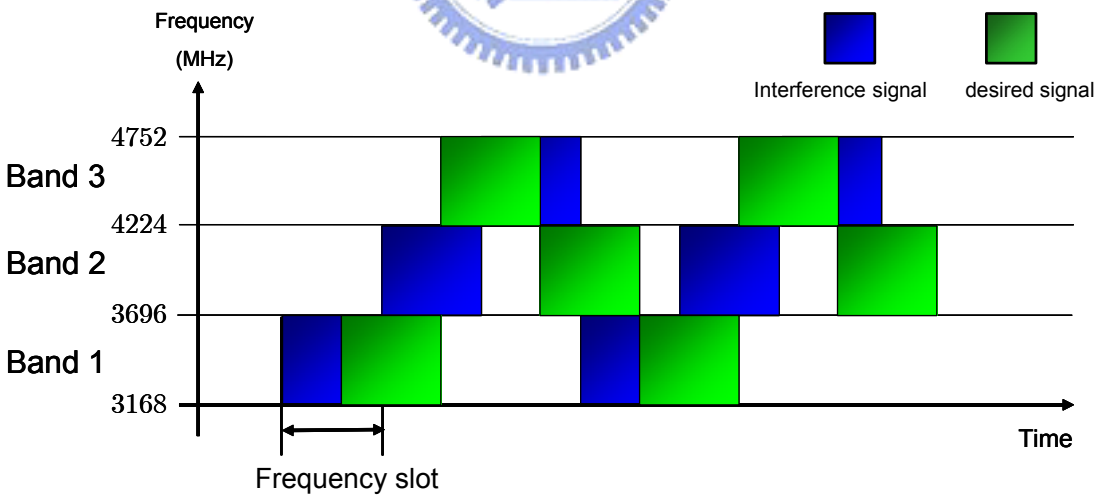

Figure 4.4: Collision property of two time–frequency interleaving codes for two piconets

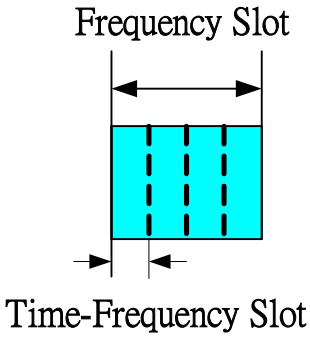

Figure 4.5: Illustration of time-frequency slots in each frequency slot

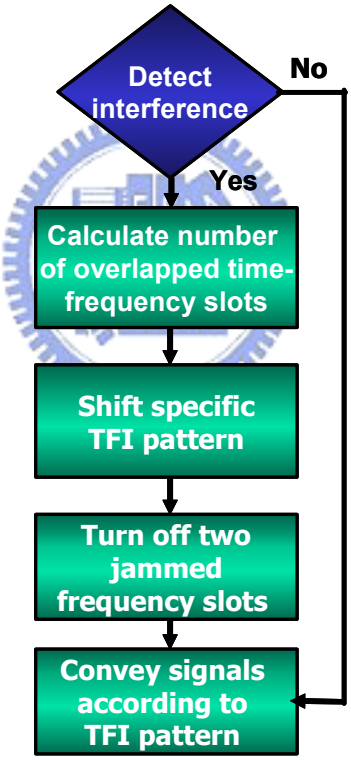

Figure 4.6: Flow chart of the interference avoidance transmission scheme

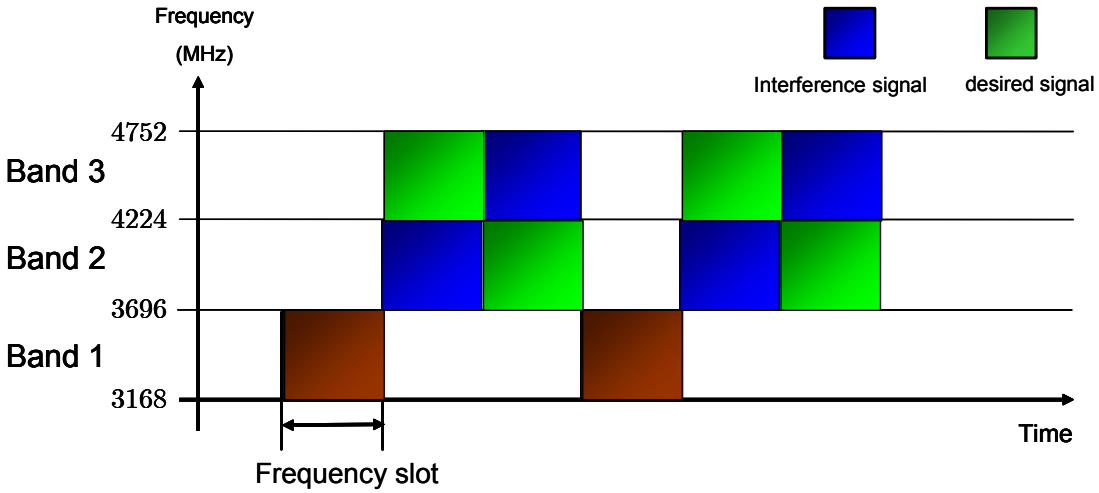

Figure 4.7: The ideal collision situation for no coordination of transmissions among two piconets

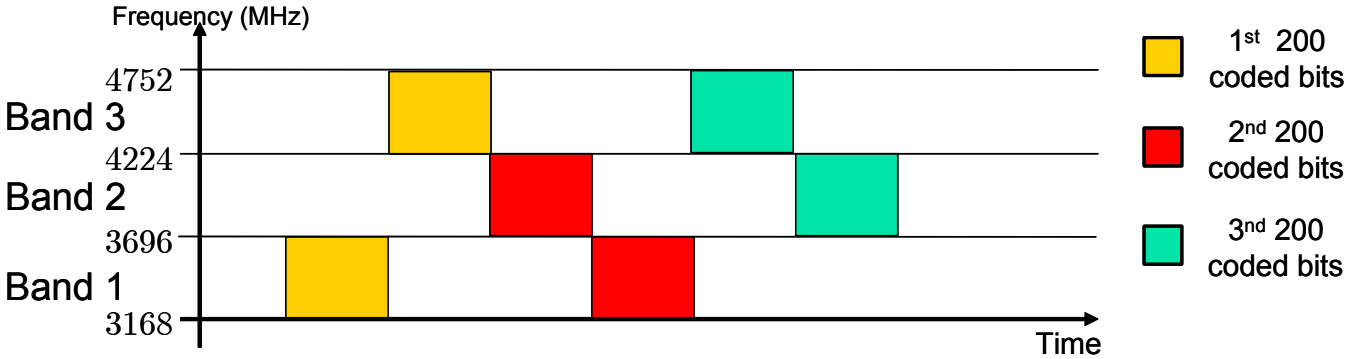

Figure 4.8: Example for the 106.7 Mbps mode of the MB OFDM system

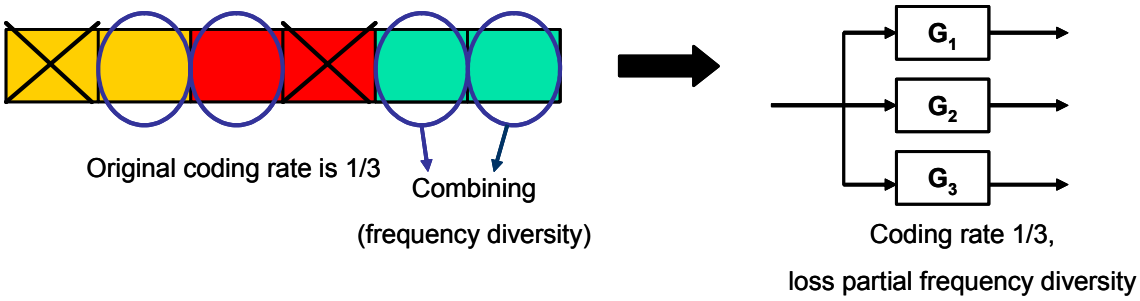

Figure 4.9: Example of transmission scheme for the 106.7 Mbps data rate mode of the MB OFDM system

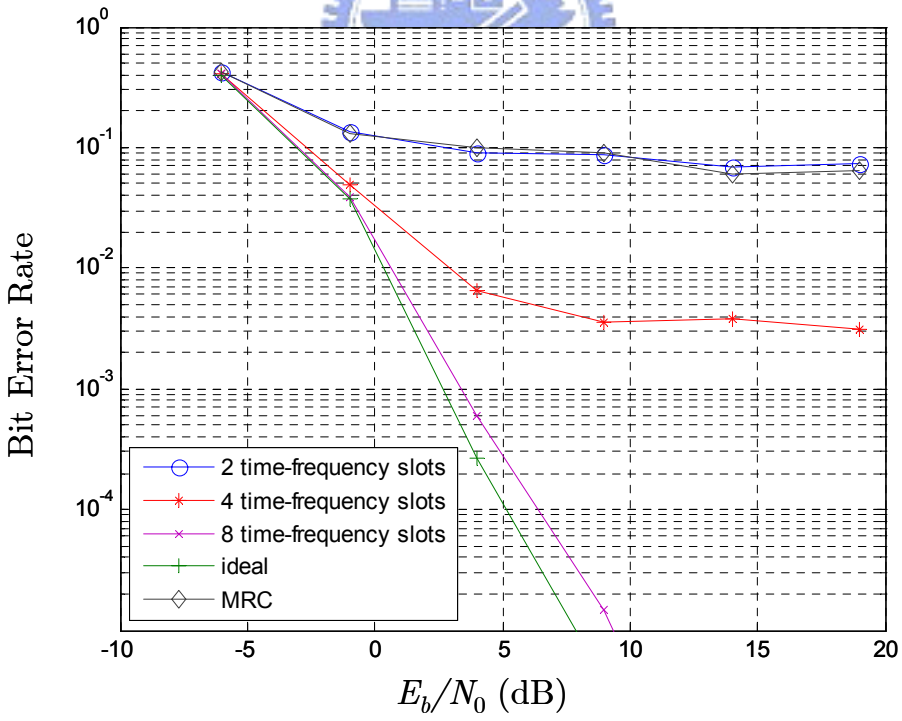

Figure 4.10: Coded BER versus E_b/N_0 for the 106.7 Mbps data rate mode of the MB OFDM system in the CM 1 channel with different number time-frequency slots (SIR = 0 dB)

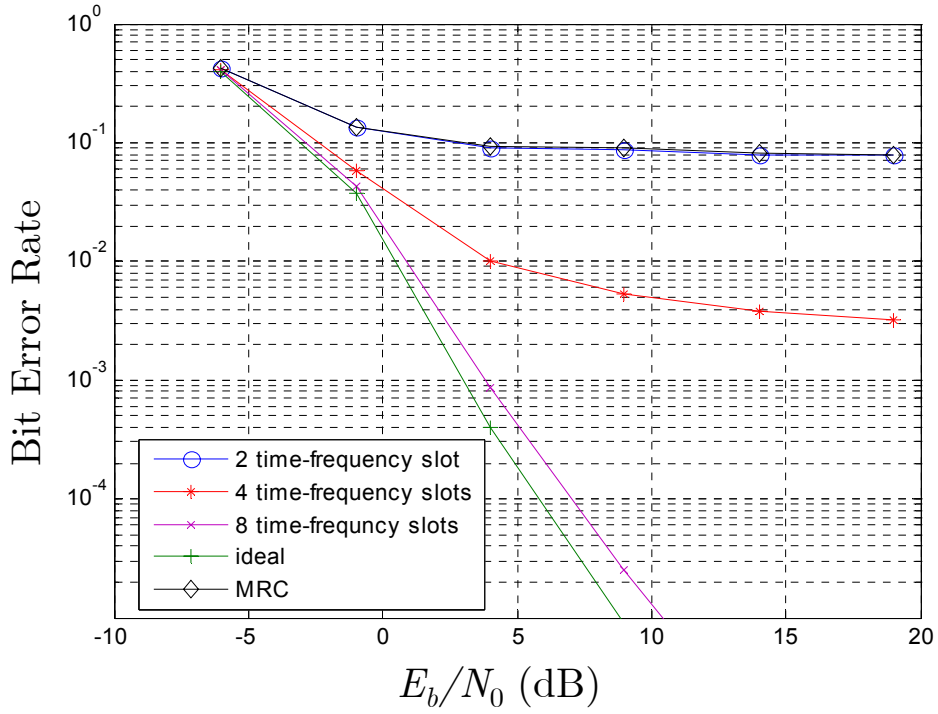

Figure 4.11: Coded BER versus E_b/N_0 for the 106.7 Mbps data rate mode of the MB OFDM system in the CM 2 channel with different number time- frequency slots (SIR=0 dB)

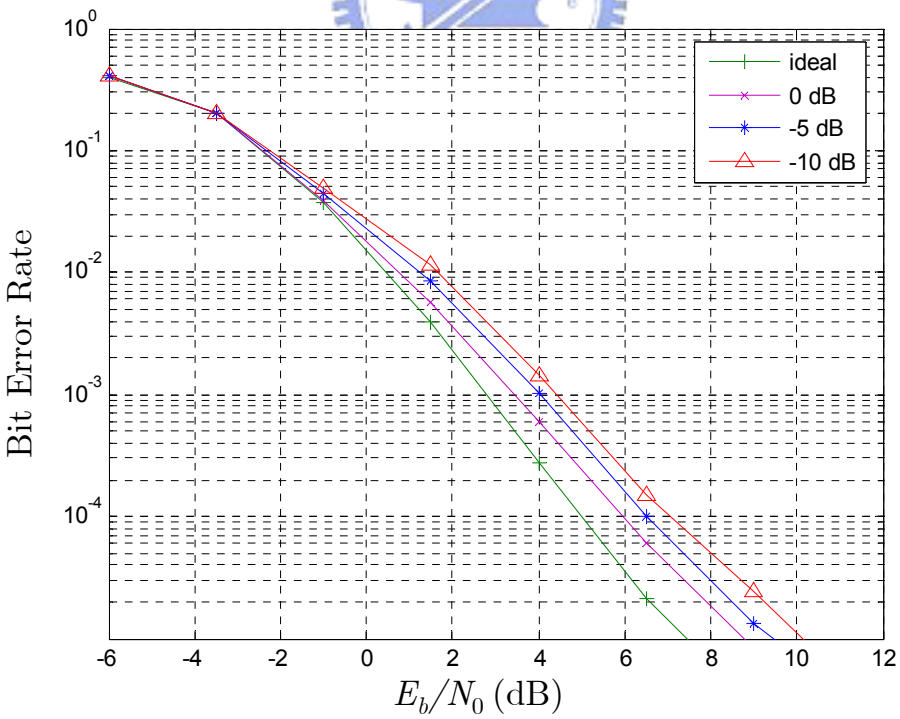

Figure 4.12: Coded BER versus E_b/N_0 for the 106.7 Mbps data rate mode of the MB OFDM system in the CM 1 channel with different SIR

Chapter 5

Conclusion

In this thesis, we propose a MB OFDM system incorporating decision-aided ICI canceller (DAIC) and interference avoidance transmission scheme. The DAIC solves the impact of ICI induced by long delay spread channels and has a lower complexity than the MMSE equalizer. The interference avoidance transmission scheme effectively mitigates degradation of performance when other piconet is present in the same area. In Chapter 2, the transmitter architecture of IEEE 802.15.3a MB OFDM system is introduced. Although the architecture is similar to that of conventional OFDM systems, the ZPP OFDM, spreading, and frequency hopping are three major characteristics different from conventional OFDM systems. In Chapter 3, we introduced the S-V model which is suitable for UWB channel environment. Then, based on the MB OFDM technical specification, we construct the receiver architecture. Synchronization and channel estimation algorithms for the MB OFDM receiver are established. The ZPP OFDM transceiver effectively eliminating the ripples in the PSD of transmitted signal is also discussed. Besides, the influence of ICI resulting from the long delay spread channel is described. We also discuss three feasible methods to improve the effect of ICI. For moderate and low data rate modes of the MB OFDM system, the receiver can mitigate the impact of ICI by MRC method. Besides, the other methods are workable for high data rate modes without

any spreading. However, the MMSE equalizer is too complex to be adopted for the MB OFDM system. The DAIC method can significantly reduce the error floors induced by the ICI and have lower complexity than MMSE equalizer. In addition, the LS channel estimation is not suitable for the CM4 channel. Because the two OFDM training symbols suffer the same influence by ICI, the LS channel estimation cannot perform reliably under the CM4 channel. We develop the DAIC method to estimate the channel impulse response. The simulation result indicates that the DAIC channel estimation effectively mitigates the effect of ICI and is more accurate than the LS channel estimation.

In Chapter 4, we first review the multiple access techniques including FDMA, TDMA, and CDMA. Then, the multiple access for intra- and inter-piconet are presented. A number of devices in a piconet share the fixed communication resource by TDMA. In the MB OFDM system, the four unique time-frequency interleaving codes are adopted to specify different piconets. However, the collisions still occur when two piconets exist at the same area. The proposed interference avoidance avoids the interference by abandoning the collided frequency slots. Then, transmitter will convey the signal in remainder frequency slots. The simulations indicate the proposed method can effectively avoid the interference and the performance of BER is close to the interference-free performance of BER.

The study presented in the thesis has discussed the receiver design for MB OFDM system and its efficacy has been verified using simulation platform. Although we present workable methods for advanced MB OFDM system, there are some challenges in implementing MB OFDM system, such as hardware and RF. Furthermore, we can investigate the performance of the interference avoidance transmission scheme in the network simulator, like NS2 and OPNET. By cross layer design, we can improve the performance of SOP further.

In practice, there are two competing UWB specifications: MB OFDM and DS-UWB systems. There are different superiorities of some system over the other. In the MB OFDM system, the obvious advantage is its capability to capture multipath energy with a simple FFT. In contrast to CDMA, the Rake correlator fingers should be used to exploit multipath diversity. The Rake correlators in CDMA based UWB receivers lead to a more complex receiver with higher power consumption. In addition, OFDM enables the designer to adapt the system to avoid using some specific bands to comply with other regulations set forth by other countries. However, the MB OFDM system still has some problems of conventional OFDM systems, such as the complexity of the transmitter and high peak-to-average power ratio (PAPR). Besides these conventional problems, the MB OFDM system has to overcome the considerably large power consumption of power amplifier and multi-nanosecond hopping time between the subbands. In spite of the advantages and drawbacks, there are some design challenges for both systems, such as frond-end LNA/mixer which have satisfied the requirements over the 7.5 GHz bandwidth set forth by FCC for UWB communications. The other notable challenge is the architectures of ADC in the UWB transceiver. They are too expensive and power consuming for UWB systems.

Although both groups are focusing on having the IEEE 802.15 standards group adopt and manage their UWB specification as a standard, it's still unclear at this point which of the specifications will win. It's very possible that both will eventually become part of the same standard, similar to 802.11a and 802.11b/g is with WLANs.

Bibliography

[1] L.Q. Yang and G.B. Giannakis, "Ultra-wideband communications: an idea whose time has come," *IEEE Signal Processing Magazine*, Vol. 21, pp. 26-54, Nov. 2004

[2] G.R. Aiello and G.D. Rogerson, "Ultra-wideband wireless systems," *IEEE Microwave Magazine*, Vol. 4, pp.36-47, June 2003

[3] FCC, "First report and order, revision of part 15 of the commission's rules reguarding ultra-wideband transmission systems," ET Docket, pp. 98-153, Feb. 2002

[4] IEEE 802.15WPAN High Rate Alternative PHY Task Group 3a (TG3a) [Online]. Available: http://www.ieee802.org/15/pub/TG3a.html

[5] WLAN Medium Access Control (MAC) and Physical Layer (PHY) Specifications, ANSI/IEEE 802.11, 1999

[6] Local and Metropolitan Area Networks, IEEE 802.3, 2002

[7] Universal Serial Bus Specification, Revision 2.0, 2000

[8] Standard for a High-Performance Serial Bus, IEEE 1394, 1995

[9] R. Fisher et al., "DS-UWB Physical Layer Submission to 802.15 Task Group 3a," *IEEE 802.15-04/0137r3*, Motorola, Inc. et al., July 2004

[10] R. Fisher et al., "DS-UWB Proposal Update for IEEE P802.15 Working Group for Wireless Personal Networks (WPANs)," *IEEE 802.15-64/04140r7*, Motorola, Inc. et al., July 2004

[11] R. Fisher et al., "Merger#2 Proposal Update for IEEE P802.15 Working Group for Wireless Personal Area Networks (WPANs)," *IEEE 802.15-64/022r0*, Motorola, Inc. et al., Jan. 2004

[12] A. Batra et al., "Multiband OFDM physical layer proposal for IEEE 802.15 Task Group 3a,"Multi-bandOFDMAlliance, Sep.2004

[13] A. Batra et al., “Design of a multiband OFDM system for realistic UWB Channel Environments,” *IEEE Transactions on Microwave Theory and Techniques*, vol. 52, pp. 2123-2138, Sep. 2004

[14] V.S. Somayazulu, J.R. Foerster, and S. Roy, “Design challenges for very high data rate UWB systems,” *Systems and Computation Conference in Processing. Asilomar Signal*, pp. 717-721, Nov. 2002

[15] A.F. Molisch, J.R. Foerster, and M. Pendergrass, “Channel models for ultrawideband personal area networks,” *IEEE Wireless Communications*, Vol. 10,pp. 14-21, Dec. 2003

[16] D. Cassioli, M.Z. Win, and A.F. Molisch, “The ultra-wide bandwidth indoor channel: from statistical model to simulations,” *IEEE Journal on Selected Areas in Communications*, Vol. 20, pp. 1247-1257, Aug. 2002

[17] IEEE 802.11-97/96, Naftali Chayat, Sep. 1997.

[18] A. Saleh and R. Valenzuela, “A Statistical Model for Indoor Multipath Propagation,” *IEEE Journal on Selected Areas in Communications*, vol. 5, no. 2, pp. 128–137, Feb. 1987.

[19] H. Hashemi, “Impulse Response Modeling of Indoor Radio Propagation Channels,” *IEEE Journal on Selected Areas in Communications*, vol. 11, no. 7, pp. 967–978, Sept. 1993.

[20] J. Terry and J. Heishkala, *OFDM wireless LANs*: *A theoretical and practical guide*, Indiana: SAMS, 2001

[21] B. Muquet et al., “Cyclic prefixing or zero padding for wireless multicarrier transmissions,” *IEEE Transactions on Communications*, Vol. 50, pp. 2136-2148, Dec. 2002

[22] A. Scaglione, G.B. Giannakis, and S. Barbarossa, “Redundant filterbank precoders and equalizers. I. Unification and optimal designs,” *IEEE Transactions on Signal Processing*, Vol. 47, pp. 1988-2006, July 1999

[23] A. Scaglione, G.B. Giannakis, and S. Barbarossa, “Redundant filterbank precoders and equalizers. II. Blind channel estimation, synchronization, and direct equalization,” *IEEE Transactions on Signal Processing*, Vol. 47, pp. 2007 - 2022, July 1999

[24] H.J. Yu, M.S. Kim; T.H. Jeori, and S.K. Lee, “Equalization scheme for OFDM systems in long delay spread channels,” *15th IEEE International Symposium on*

PIMRC, Vol. 2, pp. 1297-1301, Sept. 2004

[25] S.P. Chen and T.R. Yao, "FEQ for OFDM systems with insufficient CP," *14th IEEE Proceedings on Personal, Indoor and Mobile Radio Communications*, Vol. 1, pp. 550-553, Sept. 2003

[26] C.G. Wang and Z. Zhou; "A new detection algorithm for OFDM system without cyclic prefix," *Proceedings of the IEEE 6th Circuits and Systems Symposium on Emerging Technologies*, Vol. 2, pp. 453-456, June 2004

[27] S. Yi and T. Lang, "Channel equalization using one-tap DFE for wireless OFDM systems with ICI and ISI," *IEEE Workshop on Signal Processing Advances in Wireless Communications*, pp. 146-149, May 1999

[28] S. Yi, "Bandwidth-efficient wireless OFDM," *IEEE Journal on Selected Areas in Communications*, Vol. 19, pp. 2267-2278, Nov. 2001

[29] N. Suzuki, H. Uehara, and M. Yokoyama, "A new OFDM demodulation method to reduce influence of ISI due to longer delay than guard interval," *The 8th International Conference on Communication Systems*, Vol. 1, pp. 239-244, Nov. 2002

[30] C.J. Park and G.H. Im, "Efficient DMT/OFDM transmission with insufficient cyclic prefix," *IEEE Communications Letters*, Vol. 8, pp. 576-578, Sept. 2004

[31] A. Jamalipour, T. Wada, and T. Yamazato, "A tutorial on multiple access technologies for beyond 3G mobile networks," *IEEE Communications Magazine*, Vol. 43,pp. 110-117, Feb. 2005

[32] P.K. James, "Overview of Draft Standard 802.15.3," *IEEE 802.15-01/508r1*, Mobilian, November 2001

[33] IEEE 802.15.3 standard, "Wireless Medium Access Control (MAC) and Physical Layer (PHY) Specifications for High Rate Wireless Personal Area Networks (WPAN)," 2003 Edition

[34] Y. Li; Molisch, A.F. Molisch; and J.Y. Zhang; "Practical approaches to channel estimation and interference suppression for OFDM based UWB communications," *Proceedings of the IEEE 6th Circuits and Systems Symposium on Emerging Technologies*, Vol. 1, pp. 21-24, June 2004

[35] E. Saberinia, and A.H. Tewfik, "Multi-user UWB-OFDM communications," *IEEE Pacific Rim Conference on Communications, Computers and Signal Processing*, Vol. 1, pp. 127-130, Aug. 2003

[36] Y.P. Seung, S. Gadi, and S.K. Yong, “Interference resilient transmission scheme for multiband OFDM system in UWB channels,” *Circuits and Systems ISCAS '04*, Vol. 5, pp. 373-376, May 2004

[37] A.J. Coulson, “Narrowband interference in pilot symbol assisted OFDM systems,” *IEEE Transactions on Wireless Communications*, Vol. 3, pp. 2277-2287, Nov. 2004

94

碩士論文

適用於多頻帶正交分頻多工系統之通道及多微網衍生干擾對抗技術

交通大學電機資訊學院
電信工程學系碩士班

洪宗樺